© 2024. Published by The Company of Biologists Ltd | Development (2024) 151, dev202936. doi:10.1242/dev.202936

RESEARCH ARTICLE

Unravelling differential Hes1 dynamics during axis elongation of mouse embryos through single-cell tracking

Yasmine el Azhar[1], Pascal Schulthess[1,‡], Marek J. van Oostrom[1,‡], Sonja D. C. Weterings[1], Wilke H. M. Meijer[1], Nobuko Tsuchida-Straeten[2,*], Wouter M. Thomas[1], Marianne Bauer[3] and Katharina F. Sonnen[1,§]

ABSTRACT

The intricate dynamics of Hes expression across diverse cell types in the developing vertebrate embryonic tail have remained elusive. To address this, we have developed an endogenously tagged Hes1-Achilles mouse line, enabling precise quantification of dynamics at the single-cell resolution across various tissues. Our findings reveal striking disparities in Hes1 dynamics between presomitic mesoderm (PSM) and preneural tube (pre-NT) cells. While pre-NT cells display variable, low-amplitude oscillations, PSM cells exhibit synchronized, high-amplitude oscillations. Upon the induction of differentiation, the oscillation amplitude increases in pre-NT cells. Additionally, our study of Notch inhibition on Hes1 oscillations unveils distinct responses in PSM and pre-NT cells, corresponding to differential Notch ligand expression dynamics. These findings suggest the involvement of separate mechanisms driving Hes1 oscillations. Thus, Hes1 demonstrates dynamic behaviour across adjacent tissues of the embryonic tail, yet the varying oscillation parameters imply differences in the information that can be transmitted by these dynamics.

KEY WORDS: Oscillations, Notch signalling, Hes1, Somitogenesis, Neuromesodermal progenitors, Neural tube

INTRODUCTION

During embryonic development, tightly regulated cell fate decisions rely on intercellular communication. Recent insights indicate that cells encode information not only through the presence but also the dynamics of signalling pathways (Sonnen and Janda, 2021). Oscillations in signalling pathways and target genes are widespread across tissues and developmental stages. Prominent among these are members of the hairy and enhancer of split (Hes) family of transcriptional repressors. Hes proteins, which are basic helix-loop-helix (bHLH) transcription factors, modulate gene expression by interacting with DNA as dimers (Sasai et al., 1992). Several of the seven Hes family members in mammalian cells are dynamically expressed in embryonic development (Ohtsuka et al., 1999; Palmeirim et al., 1997; Sasai et al., 1992; Wu et al., 2003; Ohtsuka et al., 2001; Kobayashi and Kageyama, 2010).

During vertebrate development, neuromesodermal progenitors (NMPs) in the tailbud (TB) give rise to both the mesodermal and neural lineages, namely the presomitic mesoderm (PSM) and the neural tube (NT), respectively (Cambray and Wilson, 2002; 2007). Hes dynamics play a crucial role in the differentiation of both PSM and NT progenitors (Shimojo et al., 2016; 2008; Hirata et al., 2002; Ohtsuka et al., 1999). The periodic segmentation of the PSM into somites, known as somitogenesis, is driven by oscillatory signalling pathways, including FGF (fibroblast growth factor), Wnt (wingless and Int-1) and Notch signalling (Bosman and Sonnen, 2022; Dequeant et al., 2006; Matsuda et al., 2020; Palmeirim et al., 1997; Niwa et al., 2011; Aulehla et al., 2003). Whereas the exact composition of the segmentation clock differs by species, Notch signalling oscillations are found in all studied vertebrates, and several Notch target genes display oscillatory expression in PSM cells (Riedel-Kruse et al., 2007; Palmeirim et al., 1997; Soza-Ried et al., 2014; Oginuma et al., 2010; Niwa et al., 2011; Venzin and Oates, 2020), including several members of the Hes gene family (Holley et al., 2002; Palmeirim et al., 1997; Bessho et al., 2001; Hirata et al., 2002).

NMPs transitioning from the TB to the NT pass through the preneural tube (pre-NT), surrounded by oscillating PSM (Delfino-Machin et al., 2005). FGF signalling prevents premature differentiation in the pre-NT, while Notch signalling supports cell proliferation (Akai et al., 2005; Semprich et al., 2022). In the anterior NT, progenitor cells continue to proliferate and differentiate into future spinal cord neurons. Whether NT progenitor cells proliferate or differentiate has been linked to oscillations in Hes1 and Hes5 that are reminiscent of their function in somitogenesis (Shimojo et al., 2008, 2016). Hes genes oscillate in progenitor cells to maintain a proliferative state (Shimojo et al., 2008; Manning et al., 2019; Biga et al., 2021; Imayoshi and Kageyama, 2014; Shimojo et al., 2016), while sustained expression has been linked to quiescence (Marinopoulou et al., 2021; Sueda et al., 2019). Despite research into Hes dynamics in the anterior NT, investigations into Hes dynamics in NMPs and pre-NT are lacking.

In this study, we delineate the dynamics of Hes gene expression in mouse development and elucidate the signalling pathways orchestrating its expression during the differentiation of NMPs along neural and mesodermal trajectories. Leveraging a newly developed homozygously viable Hes1 reporter mouse line, generated through the endogenous tagging of the gene locus with a rapidly maturing yellow fluorescent protein, we thoroughly quantify Hes1 dynamics in the PSM, TB and pre-NT regions of the embryonic tail. Through single-cell tracking, we discern distinct Hes1 dynamics between the PSM and pre-NT. Further investigation

[1]Hubrecht Institute-KNAW (Royal Netherlands Academy of Arts and Sciences), University Medical Center Utrecht, Utrecht 3584, The Netherlands. [2]European Molecular Biology Laboratory (EMBL), 69117 Heidelberg, Germany. [3]Department of Bionanoscience, Kavli Institute of Nanoscience Delft, Technical University of Delft, Van der Maasweg 9, 2629 HZ Delft, The Netherlands.
‡These authors contributed equally. *Present address: Institut für Humangenetik, Universitätsklinikum Heidelberg, 69117 Heidelberg, Germany.

§Author for correspondence: k.sonnen@hubrecht.eu

P.S., 0000-0002-7768-8507; W.H.M.M., 0000-0003-3962-2854; M.B., 0000-0002-1191-986X; K.F.S., 0000-0002-2902-9419

Handling Editor: James Briscoe
Received 8 April 2024; Accepted 22 August 2024

Development (2024) 151, dev202936. doi:10.1242/dev.202936

into Hes1 dynamics reveals disparate responses of PSM and pre-NT cells to signalling pathway perturbations. Thus, our new endogenous reporter mouse line, combined with recently available single-cell tracking software, allows us to uncover previously unquantified dynamics in single cells of the mouse embryonic tail.

RESULTS

Generation of a Hes1-Achilles mouse line to study signalling dynamics in the posterior embryonic tail

To investigate Hes dynamics in the developing mouse embryo, we first clarified which Hes genes were expressed in the PSM, TB and, in particular, the pre-NT. The last is defined as the tube-like Pax6-negative region emanating from the TB, which lies next to the PSM (Fig. 1A,B) (Semprich et al., 2022; Akai et al., 2005). To this end, we performed *in situ* hybridization and hybridization chain reactions (Choi et al., 2018) (Fig. S1). Expression of Hes7 and Lfng (lunatic fringe), key components of the segmentation clock (Morales et al., 2002; Lázaro et al., 2023; Harima et al., 2013; Bessho et al., 2003, 2001), was restricted to the PSM and TB (for Hes7) or PSM (for Lfng) (Fig. S1A,B,D). In contrast, both Hes1 and Hes5 were present in the TB, the PSM and the pre-NT, with highest expression levels in the pre-NT and TB (Figs 1C and S1C,D) (Hatakeyama et al., 2004) (also see MAMEP database, http://mamep.molgen.mpg.de). Thus, Hes1 and Hes5 are not limited to PSM, but are also expressed in the TB and pre-NT of the embryonic tail.

For further analysis into the dynamics of Hes genes, we then focused on Hes1, which shows a more localized expression to the

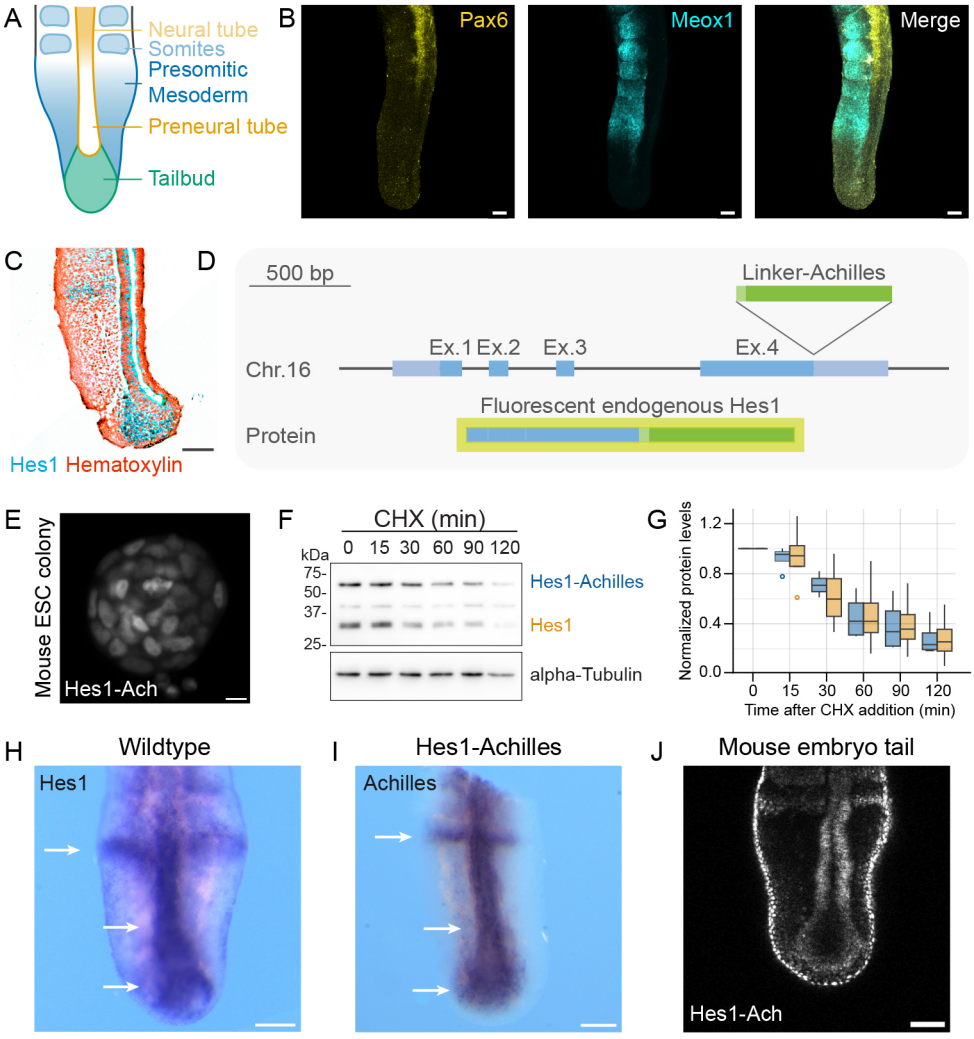

Fig. 1. Generation of a Hes1-Achilles mouse line to study Hes dynamics in the posterior embryonic tail. (A) Schematic representation of the posterior mouse embryonic tail. The tailbud (green) differentiates into presomitic mesoderm (PSM, blue), which gives rise to somites (light blue) and the preneural tube (pre-NT, yellow), which differentiates into the neural tube (NT, light yellow). (B) Representative images of a E10.5 embryonic tail stained by hybridization chain reaction for the mesodermal marker Meox1 and neural marker Pax6. Scale bars: 100 µm. (C) A 5 µm section of an E10.5 embryonic tail with *in situ* hybridization for Hes1 (as shown in Fig. S1F). Scale bar: 100 µm. (D) Schematic representation of the tagging strategy for the Hes1-Achilles mouse line. Hes1 was endogenously tagged with linker-Achilles. (E) Representative image of a mouse ESC colony expressing the Hes1-Achilles construct. There is variable expression in the different cell types. Scale bar: 10 µm. (F,G) ESCs were treated with cycloheximide (CHX) for the indicated durations. The 0 min timepoint was treated with DMSO as a control. Cells were lysed and protein levels analysed by western blotting. Levels of untagged and tagged Hes1 were quantified by normalizing to alpha-tubulin and the 0 min control (n=4). Representative blots are shown in F and the quantification in G. Bar indicates the median, boxes indicate the 25th and 75th percentiles, and whiskers indicate 1.5×IQR. Individual values are shown in Fig. S2M. (H,I) Representative images of tails of an E10.5 embryo with *in situ* hybridization for Hes1 (H) (as shown in Fig. S1F) and Achilles (I). Arrows highlight the expression pattern in the posterior embryonic tail. Scale bar: 100 µm. (J) Representative image of an E10.5 embryonic tail expressing the Hes1-Achilles reporter. Scale bar: 100 µm.

Development (2024) 151, dev202936. doi:10.1242/dev.202936

neural lineage and PSM of the developing embryo than the ubiquitously expressed Hes5 (MAMEP database). To be able to quantify expression levels over time, we generated a new Hes1 mouse line (Fig. 1D-J, Fig. S2). Building on previous approaches (Yoshioka-Kobayashi et al., 2020; Niwa et al., 2007; Masamizu et al., 2006; Marinopoulou et al., 2021), we endogenously tagged Hes1 with Achilles, a fast-maturing fluorescent protein (Yoshioka-Kobayashi et al., 2020) (Fig. 1D). We placed Achilles at the C-terminal side of Hes1 opposite the DNA-binding bHLH domain of Hes1 (Sasai et al., 1992). We separated Achilles and Hes1 by a flexible linker, reasoning that this should allow interaction of Hes1 via its C-terminal WRPW motif with the Groucho/TLE family of transcriptional repressors (Jennings et al., 2006; Fisher et al., 1996). Structure of the fusion protein was assessed for accessibility of the WRPW motif and bHLH domain using Alphafold (Jumper et al., 2021; Varadi et al. 2024) (Fig. S2J,K).

While Hes1 knockout mice die directly after birth (Suzuki et al., 2005; Jensen et al., 2000), homozygous Hes1-Achilles mice were born at Mendelian ratio (offspring of eight heterozygous breedings: 17 wild type, 34 heterozygous and 16 homozygous), and were viable and fertile. Moreover, Hes1-knockout mice show premature differentiation of Paneth cells in the intestine (Suzuki et al., 2005). However, we did not detect differences in intestinal morphology or Paneth cell number in the small intestine when comparing wild-type and Hes1-Achilles homozygous mice (Fig. S2L,M). We next confirmed that Hes1 dynamics and, in particular, protein turnover were not altered by tagging. To this end, we compared the half-life of tagged versus untagged Hes1 protein in embryonic stem cells (ESCs) heterozygous for Hes1-Achilles (Fig. 1E) upon translation inhibition and found these to be comparable (Figs 1F,G and S2N,O). Finally, we investigated the expression pattern of Hes1-Achilles. When comparing mRNA staining of Hes1 in wild-type embryos and Achilles in Hes1-Achilles embryos, the expression patterns corresponded (Figs 1H,I and S2P,Q). At the protein level, Hes1-Achilles expression had the expected pattern, with high expression levels in the pre-NT and stripes in the forming somites (Fig. 1J). Thus, we successfully generated an endogenous Hes1-Achilles reporter mouse line with maintained Hes1 functionality and dynamics.

Hes1 expression is dependent on Notch signalling in the posterior embryonic tail

We next addressed whether Hes1 expression was solely dependent on Notch signalling or also on other pathways, as suggested previously for Hes7 (Niwa et al., 2007). To test this, we had to culture E10.5 embryonic tails *ex vivo*. However, standard embryo culture protocols (Lauschke et al., 2013) needed to be optimized for survival of the NT by testing different media compositions (Fig. 2A; see Materials and Methods). In standard embryo culture medium, cleaved caspase 3 expression levels were significantly higher than in uncultured embryos at embryonic day E11.5, especially in the pre-NT and NT (Fig. 2A,B). The tube was often filled with dead cells or disintegrated entirely. In contrast, in embryonic tails cultured in neurobasal medium (see further details in the Materials and Methods), the number of apoptotic cells was not increased compared with uncultured tails. Furthermore, the NT maintained its morphology and proliferative state (Fig. 2A,C). This suggests that the pre-NT is viable in the neurobasal medium. Even though somites were less organized in neurobasal medium than in control samples (Fig. 2A), we did not observe differences in the well-studied dynamics of the segmentation clock using the segmentation clock reporter line LuVeLu (Aulehla et al., 2008). Oscillation dynamics as well as the regression of the oscillating field, a sign of differentiation, were similar between embryonic tails cultured in the different media (Fig. S3A-D). Thus, the dynamics of the segmentation clock were maintained. The optimized culture conditions of embryonic tails now allows the investigation of signalling dynamics in PSM, TB and pre-NT *ex vivo*.

We initially tested how pathway perturbation affected Hes1-Achilles expression levels. Notch inhibition using the γ-secretase inhibitor DAPT led to a drop in Hes1-Achilles expression levels within 3 h (Fig. 2D,E), which was comparable with the effect of Notch inhibition on the reporter Achilles-Hes7 (Yoshioka-Kobayashi et al., 2020) (Fig. S3E,F). Besides Notch signalling, we also focused on Wnt and FGF signalling, as gradients of these morphogens, including the respective downstream targets Axin2 and Dusp4, are present in the embryonic tail and pre-NT (Fig. S3G,H). We therefore perturbed embryonic tails with small molecules inhibiting these pathways, using the porcupine inhibitor IWP2 to inhibit Wnt signalling (Fig. S3I-K) and SU5402, a small molecule inhibitor against the FGF receptor, to inhibit FGF signalling (Fig. S3L-N). As expected, both inhibitors lead to a rapid regression of the oscillating field in the PSM (Fig. S3K-N). Inhibiting either did not lead to an immediate (IWP2) or consistent (SU5402) drop in signal, suggesting that these pathways do not have a direct effect on Hes1 expression levels. Thus, Hes1 expression in the posterior embryonic tail is driven by Notch signalling.

Population-wide Hes1 dynamics differ between TB, pre-NT and PSM

Subsequently, we carefully quantified Hes1-Achilles dynamics in the different regions of the embryonic tail (TB, PSM and pre-NT) (Figs 3A-G and S4, Movie 1). We quantified dynamics in the TB region (Fig. 3D), which includes the NMPs but presumably also some posterior PSM cells. Expression levels differed between all regions, in particular the pre-NT showed higher levels compared with the PSM region (Fig. 3H). In both the PSM and TB region, we detected oscillations over time (Fig. 3C,E). In contrast, Hes1-Achilles expression in the pre-NT region was dynamic, albeit noisier and showed less apparent oscillations over time (Fig. 3G). When analysing the period using wavelet transform (Schmal et al., 2022), there was a slight increase in the TB region compared with the PSM region (Fig. 3I). A trend towards the elevated period was also observed for the pre-NT region. Furthermore, the amplitude of the PSM region was significantly higher than in the pre-NT and TB regions (Fig. 3J). Throughout the study, we have quantified the amplitude after normalization to the mean intensity of a track, i.e. the amplitude should be considered relative to the absolute intensity. Finally, whereas kymographs revealed travelling waves of Hes1-Achilles expression levels in the PSM region (see asterisk in kymograph), no clear population-wide wave patterns were detected in the pre-NT region (Figs 3K and S3O). Overall, the data suggest that Hes1 is dynamic in the different regions of the mouse embryonic tail. However, Hes1 expression in the pre-NT seem to be noisier and less oscillatory compared with the PSM.

Hes1 is oscillatory in single cells of the pre-NT

There are two possible reasons for not finding clear population-wide Hes1 oscillations or travelling waves in the pre-NT region: (1) there are no oscillations; (2) single cells oscillate but are not synchronized with each other. To test the latter, we performed a 2D spread-out experiment (Lauschke et al., 2013) combined with mosaic labelling of nuclei that allowed us to track cells and quantify Hes1-Achilles expression in single cells (Figs 4A-E, S5 and S6; Movie 2). When posterior embryonic tail-tips are cultured on fibronectin-coated dishes, tissue spreads and cells grow in a quasi-monolayer (Lauschke et al., 2013), which facilitates single-cell tracking.

Development (2024) 151, dev202936. doi:10.1242/dev.202936

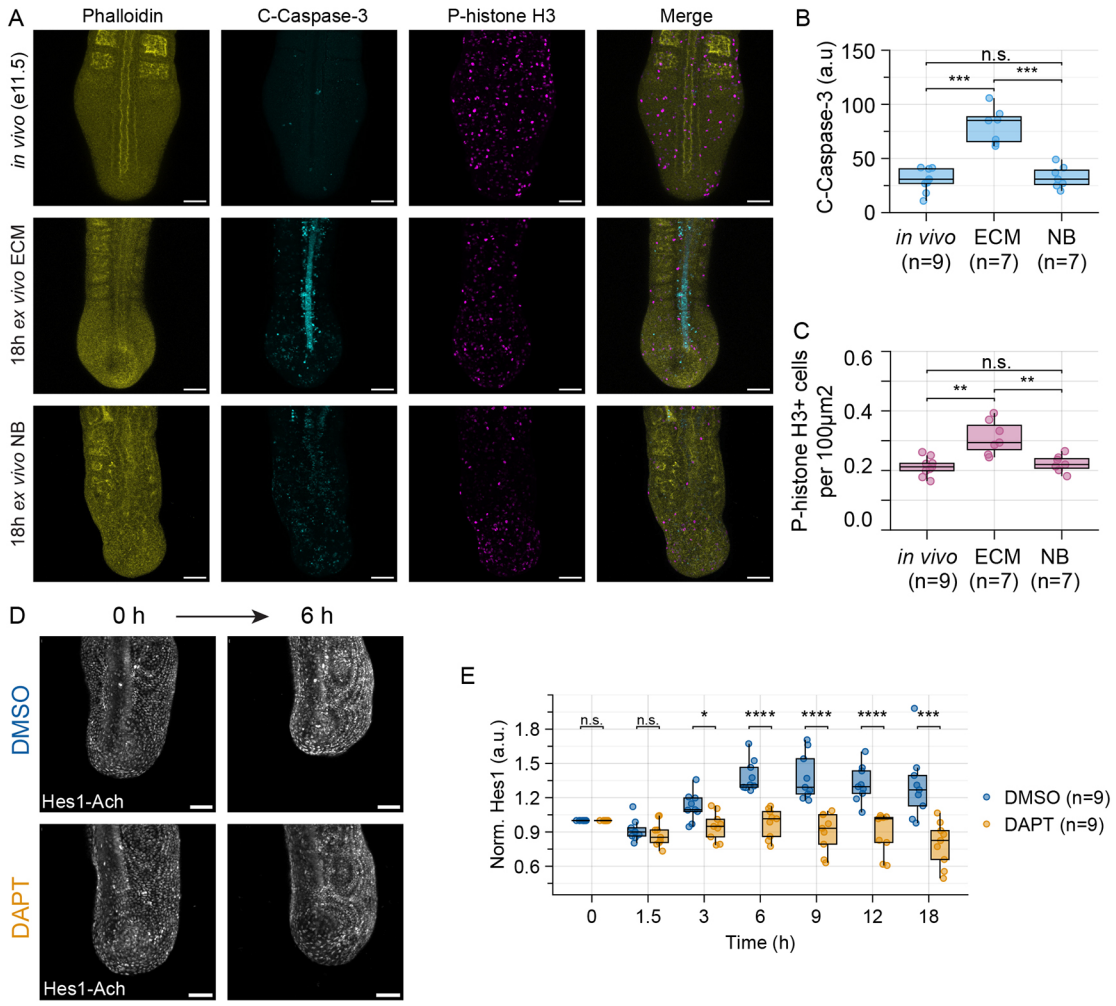

Fig. 2. Inhibition of Notch signalling results in a decrease in Hes1-Achilles levels in *ex vivo* cultured E10.5 embryonic tails. (A-C) Comparison of different culture media to optimize the survival of the pre-NT *ex vivo*. Embryonic tails were cultured *ex vivo* for 18 h in embryo culture medium (ECM) or neurobasal (NB) medium and compared with uncultured (*in vivo*) E11.5 embryos. Immunostaining against cleaved-caspase 3 (C-Caspase 3, apoptosis), phospho-histone H3 (P-histone H3, mitosis) and counterstaining with phalloidin were performed. (A) Representative images. Scale bars: 100 µm. (B) The intensity of cleaved-caspase 3 signal in the embryonic tail. (C) The number of mitotic cells in the pre-NT (see Materials and Methods for further details). (D,E) E10.5 embryonic tails were cultured *ex vivo* and incubated with DMSO control or the gamma-secretase inhibitor DAPT (10 µM). Hes1-Achilles intensity (normalized to the first timepoint) was measured over time. (D) Representative images. Scale bars: 100 µm. (E) The quantification of Hes1-Achilles intensity in the embryonic tail. Bar indicates the median, boxes indicate the 25th and 75th percentiles, and whiskers indicate 1.5×IQR. Dots in boxplots represent individual data points. **P*<0.05, ***P*<0.01, ****P*<0.001, *****P*<0.0001 (Mann–Whitney U-test).

Staining for neural and mesodermal markers confirmed the presence and survival of PSM and neural cell types, when culturing in neurobasal medium (Fig. S5A,B). PSM and pre-NT regions displayed similar Hes1 dynamics when analysed at population level (Fig. S5C,D), as was observed for the respective region in growing embryonic tails (Figs 1 and 3). Hes1-Achilles expression was higher in pre-NT than PSM cells, the latter of which slightly increased in intensity upon differentiation to somites (Fig. 4F). Interestingly, oscillatory Hes1-Achilles dynamics were found in both PSM and pre-NT cells (Fig. 4B-E). Wavelet analysis indicated similar wavelet power distributions for PSM and pre-NT cells (Fig. S6B). Likewise, the periods and amplitudes were similar, even though the amplitudes in pre-NT cells were slightly reduced (Fig. 4G,H). The discrepancy between amplitude at population (Fig. 3J) and single-cell level (Fig. 4H) supports the hypothesis that Hes1 dynamics are less synchronized between neighbouring pre-NT cells.

Using Fourier transform to analyse the dynamics, similar periods were obtained (Figs 4I,J and Fig. S5E,F). Comparison of Fourier spectra of individual cells indicated that Hes1-Achilles dynamics were noisier in pre-NT than in PSM cells, as PSM cells mostly showed one main peak at 2.5 h and pre-NT cells showed multiple peaks around 2-4 h (Figs 4I,J and S6C). As a measure of variability, we determined the full width at half maximum (FWHM) for the period quantification (Fig. S5G), which was 0.5 for the PSM and 1.6 for the pre-NT. The coefficient of variation for periods was 0.1 and 0.2 for PSM and pre-NT cells, respectively. Finally, to quantify synchronization between cells of a tissue, we calculated the Kuramoto order parameter (Sanchez et al., 2022) between oscillations of single cells per embryonic tissue, which was approx. 0.8 for PSM and 0.45 for pre-NT cells (Fig. 4K). Thus, like PSM cells, single cells in the pre-NT show Hes1 oscillations, albeit with higher variability and lower synchronization.

Hes1 oscillates in NMPs that are driven by Notch signalling

As pre-NT and PSM both arise from the NMPs, we next sought to quantify Hes1 dynamics in NMPs. The 2D spread-out experiments

Development (2024) 151, dev202936. doi:10.1242/dev.202936

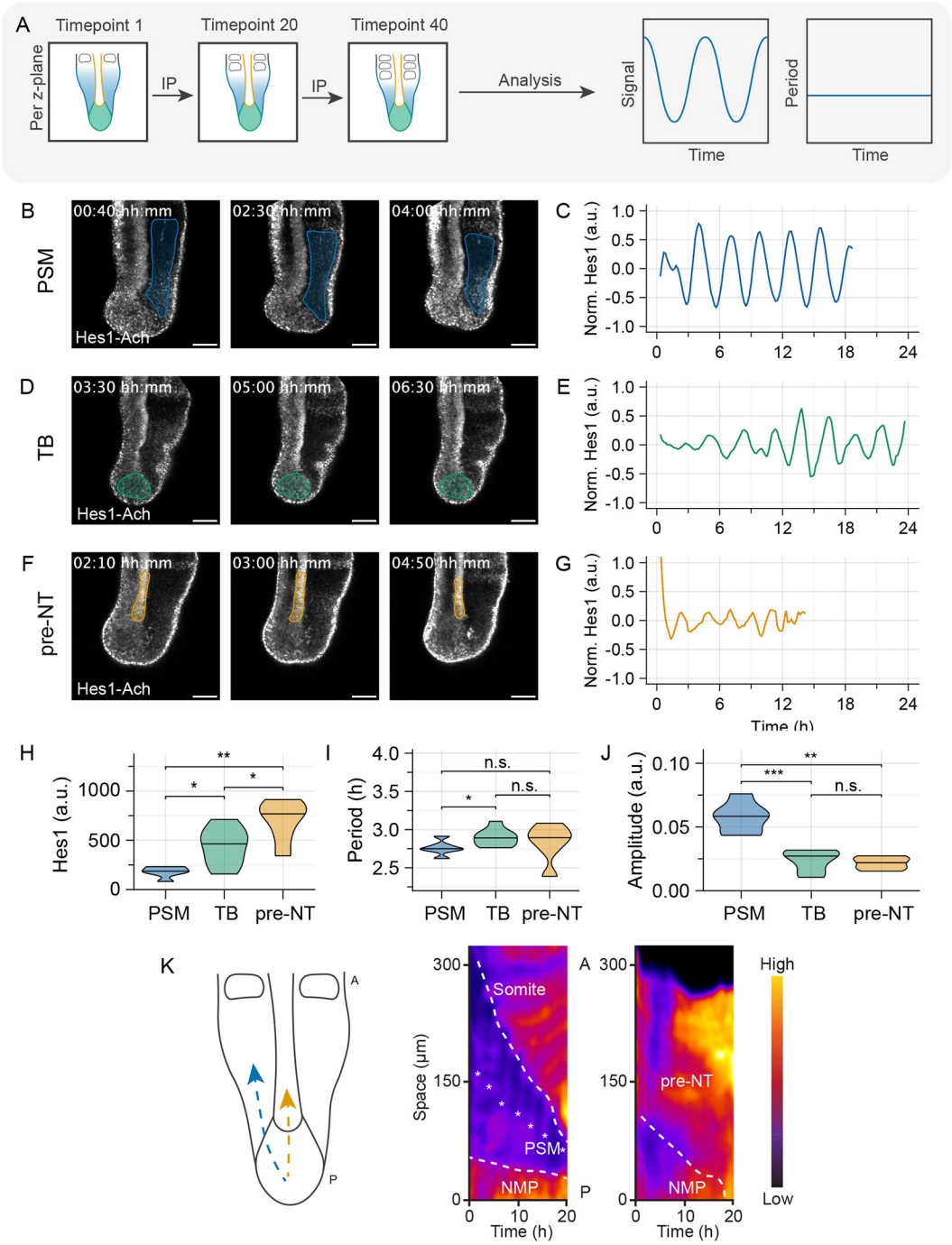

Fig. 3. Preneural tube and tailbud region in *ex vivo* cultured E10.5 embryonic tails show low amplitude oscillations at population level. (A) Embryonic tails were cultured *ex vivo* and Hes1-Achilles intensity measured by fluorescence real-time imaging (corresponding to correctly positioned control samples from Fig. 2, Fig. S3). Regions of interest were selected manually and interpolated (IP) between timepoints. Hes1-Achilles dynamics were then quantified by wavelet transform (single timeseries data shown in Fig. S4). (B,C) Quantification of Hes1-Achilles dynamics in the presomitic mesoderm (PSM) region. Representative snapshots are shown in B and the corresponding time series data (mean-normalized) of single PSM region (as indicated in B) are shown in C. (D,E) Quantification of Hes1-Achilles dynamics in the tailbud (TB) region. Representative snapshots are shown in D and the corresponding time series data (mean-normalized) of single TB region (as indicated in D) are shown in E. (F,G) Quantification of Hes1-Achilles dynamics in the preneural tube (pre-NT) region. Representative snapshots are shown in F and the corresponding time series data (mean-normalized) of single pre-NT region (as indicated in F) are shown in G. (H) Quantification of absolute Hes1-Achilles intensity in the different regions (PSM, n=6 tails; TB, n=8 tails; pre-NT, n=6 tails). (I,J) Quantification of the period (I) and amplitude (J) by wavelet transform. (K) Left panel: kymographs of Hes1-Achilles dynamics were generated along the arrows indicated (PSM in blue and pre-NT in yellow) from the posterior (P) to the anterior (A) region of the embryonic tail. Right panel: representative kymographs for PSM and pre-NT are shown. The Hes1-Achilles wave is indicated by asterisks. Scale bars: 100 µm. *P<0.05, **P<0.01, ***P<0.001 (Mann–Whitney U-test).

(Fig. 4) did not allow us to unequivocally identify NMPs. Therefore, we analysed Hes1-Achilles dynamics in NMPs by *in vitro* differentiation from ESCs derived from Hes1-Achilles mice, applying a previously published protocol (Fig. 5A) (Gouti et al., 2014). To identify embryonic and neural fate, while quantifying Hes1-Achilles expression levels over time, we added a Sox2-H2B-iRFP

Development (2024) 151, dev202936. doi:10.1242/dev.202936

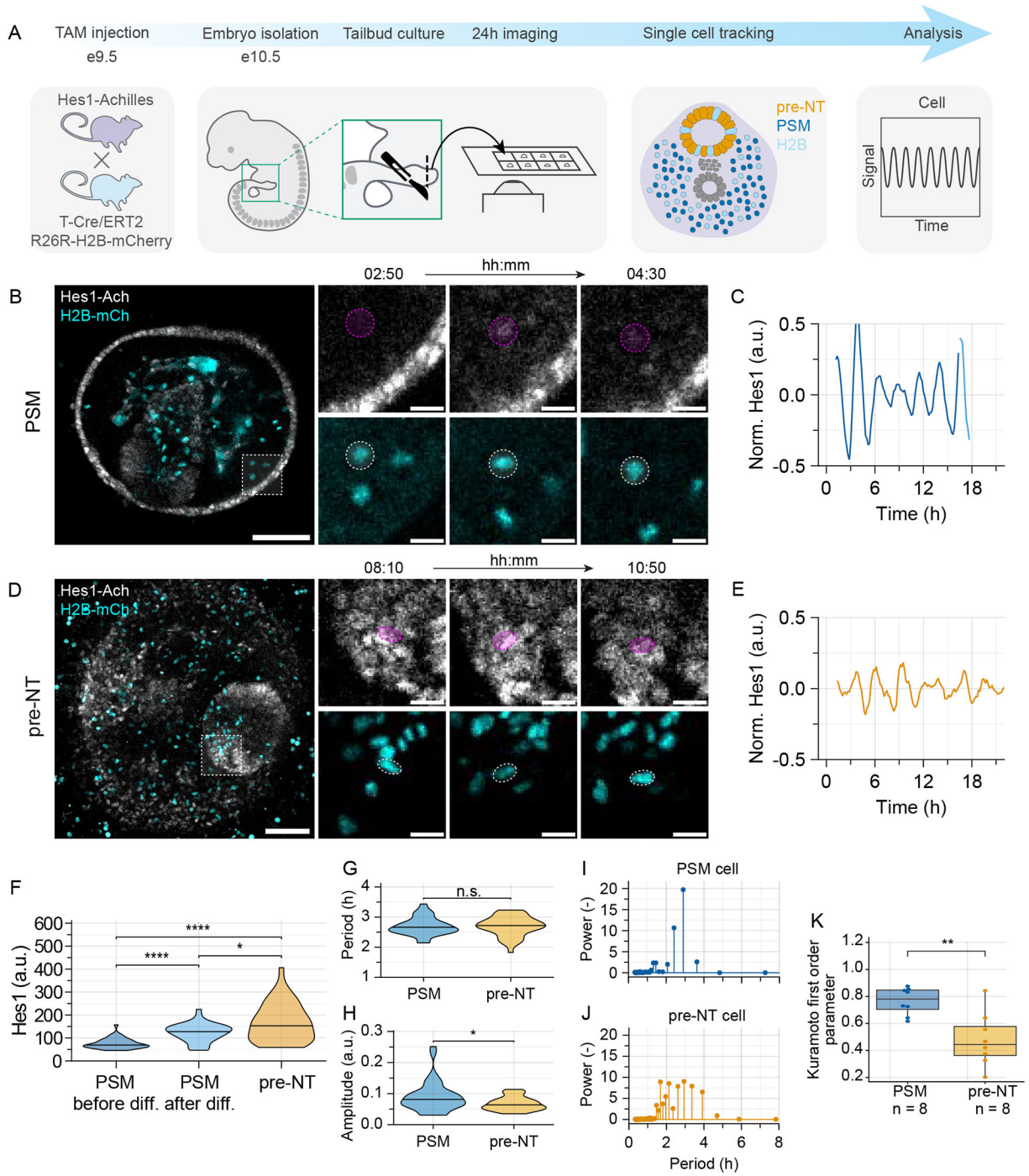

Fig. 4. Both presomitic mesoderm and preneural tube cells show Hes1 oscillations at single-cell level. (A) Sparse labelling with H2B-mCherry was induced by injection of tamoxifen (TAM). Embryonic tail tips were cultured *ex vivo* on fibronectin-coated dishes. Hes1-Achilles and H2B-mCherry intensities were measured by fluorescence real-time imaging. Single cells were tracked semi-automatically to quantify Hes1-Achilles dynamics (all single-cell timeseries data are shown in Fig. S6A). (B,C) Quantification of Hes1-Achilles dynamics in presomitic mesoderm (PSM) cells. Representative snapshots are shown in B. Representative time series data (mean-normalized) of a single PSM cell (blue) is shown in C. A differentiated PSM cell is indicated by light-blue colour. (D,E) Quantification of Hes1-Achilles dynamics in preneural tube (pre-NT) cells. Representative snapshots are shown in D. Representative time series data (mean-normalized) of a single pre-NT cell is shown in E. (F) Quantification of absolute Hes1-Achilles intensity in the different regions (diff.=differentiation) of the embryonic tail. (G,H) Quantification of the period (G) and amplitude (H) by wavelet transform. (I,J) Representative Fourier spectra of a single PSM (I) or pre-NT (J) cell are shown. Note that there is one dominant peak at 2.5 h for PSM, but not one dominant peak for pre-NT (all Fourier spectra are shown in Fig. S6B). (K) The Kuramoto order parameter was quantified for all cells tracked per region and sample. Bar indicates the median, boxes indicate the 25th and 75th percentiles, and whiskers indicate 1.5×IQR. Scale bars: 100 µm. **P*<0.05, ***P*<0.01, *****P*<0.0001 [Mann–Whitney U-test (F-H) and unpaired *t*-test (K)]. PSM cells, *n*=39; pre-NT cells, *n*=40.

reporter (‘Sox2-iRFP’) into Hes1-Achilles cells by endogenously tagging Sox2. Based on immunostainings and previous literature, we defined the NMP window between 56 and 72 h (Figs 5A and Fig. S7A) (Metzis et al., 2018; Gouti et al., 2014). When analysing Hes1-Achilles dynamics at the population level, oscillations resembled the appearance and amplitude of the TB region in *ex vivo*

Development (2024) 151, dev202936. doi:10.1242/dev.202936

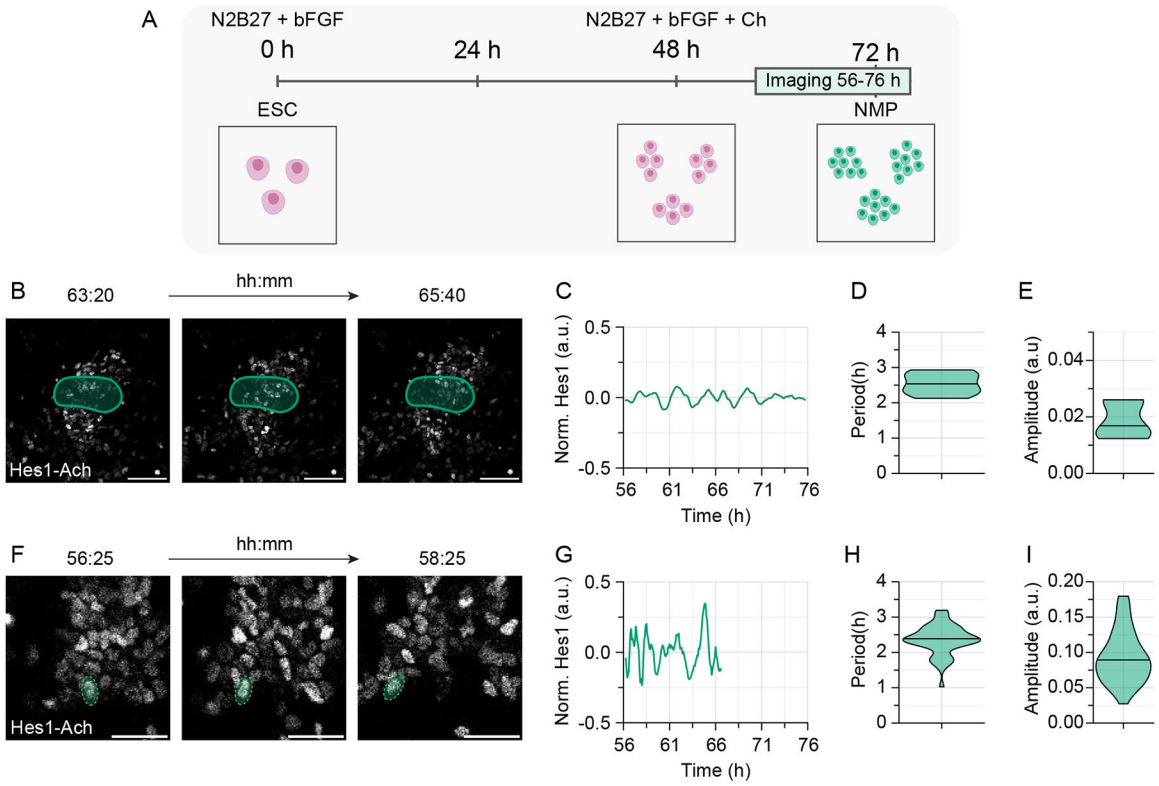

Fig. 5. Hes1 shows noisy oscillations in *in vitro* differentiated neuromesodermal progenitors. (A) Mouse embryonic stem cells (ESCs) were differentiated *in vitro* to neuromesodermal progenitors (NMPs). Hes1-Achilles intensity was measured by fluorescence real-time imaging at 56-76 h of differentiation. (B-E) Quantification of Hes1-Achilles dynamics in whole NMP colonies (n=8). Representative snapshots are shown in B. Time series data (mean-normalized) of representative colony in NMP conditions (region of interest highlighted in B) is shown in C. Scale bars: 100 µm. (D,E) Quantification of the period (D) and amplitude (E) by wavelet transform. (F-I) Quantification of Hes1-Achilles dynamics in single cells in NMP conditions (n=46). Single cells were tracked manually to quantify Hes1-Achilles dynamics. Representative snapshots are shown in F. Representative time series data (mean-normalized) of a cell in NMP conditions (highlighted in F) is shown in G. (H,I) Quantification of the period (H) and amplitude (I) by wavelet transform. Scale bars: 50 µm. Data correspond to control data in Fig. S7B-E.

embryonic tails, albeit with a reduced period (Figs 5B-E and 3D,E). We next tracked single cells under NMP conditions and quantified Hes1-Achilles dynamics (Fig. 5F-I). Hes1-Achilles expression was dynamic in NMPs with a period of around 2.5 h (Fig. 5H). The oscillations were variable with low amplitude (Fig. 5G,I). When perturbing Notch signalling using the inhibitor DAPT, we detected a dose-dependent decrease of Hes1-Achilles expression levels, but no apparent effect on period or amplitude of Hes1-Achilles dynamics (Fig. S7B-E). When we differentiated NMPs further towards the mesodermal or neural lineage (Fig. S7F-P), cells displayed Notch-dependant Hes1 dynamics, in particular period and amplitude, at population level corresponding to those found *ex vivo* (Fig. 3I,J). Thus, cells differentiated towards NMPs show variable oscillations in Hes1 expression levels that are Notch dependent.

Induced differentiation to neural tube by FGF inhibition results in Hes1 dynamics with increased amplitude in the pre-NT

Previous studies have highlighted the function of Hes dynamics in the anterior NT (Sueda et al., 2019; Bansod et al., 2017; Hirata et al., 2002; Ohtsuka et al., 2001; Biga et al., 2021; Manning et al., 2019). Therefore, we asked how Hes1 dynamics changed upon induced differentiation. As FGF inhibition induces differentiation of pre-NT to NT (Semprich et al., 2022; Delfino-Machin et al., 2005; Patel et al., 2013) and PSM to somite (Dubrulle and Pourquie, 2004; Dubrulle et al., 2001), we inhibited FGF activity in 2D spread-out cultures using SU5402 (Figs 6, S8 and S9). As expected, FGF inhibition led to a rapid regression of the oscillating field in the PSM, which indicated induced differentiation and confirmed effectiveness of the inhibitor (Fig. S8A). In agreement with changes of Hes1 expression levels from ‘posterior’ to ‘anterior’ PSM (Fig. 4F), Hes1-Achilles expression levels at the population level were increased in the PSM region, while the amplitude and period remained unchanged (Fig. S8B-D). In contrast, Hes1-Achilles expression levels were slightly decreased in the pre-NT region upon FGF inhibition with the period and amplitude also being unaffected (Fig. S8E-G).

In single PSM cells, FGF inhibition had a similar effect on Hes1-Achilles dynamics at the population level, with increased absolute expression levels, while the amplitude and period were maintained (Fig. S8H-J). In contrast, FGF signalling inhibition had a different effect on Hes1-Achilles dynamics in pre-NT cells: absolute expression levels and the oscillation period remained similar (Figs 6A-D and S8K,L), whereas the amplitude increased (Figs 6E and Fig. S8M).

It has been shown recently that expression of the Notch ligand Delta-like 1 (Dll1) begins to oscillate in the NT, adjacent to the last-formed somites (Shimojo et al., 2016). To test whether differentiation induced by FGF inhibition might have led to changes in Dll1 expression in 2D cultures, we quantified Dll1 by immunostaining. However, we did not detect changes in Dll1 expression levels in the Sox2-positive cell population upon FGF inhibition (Figs 6F,G and

Development (2024) 151, dev202936. doi:10.1242/dev.202936

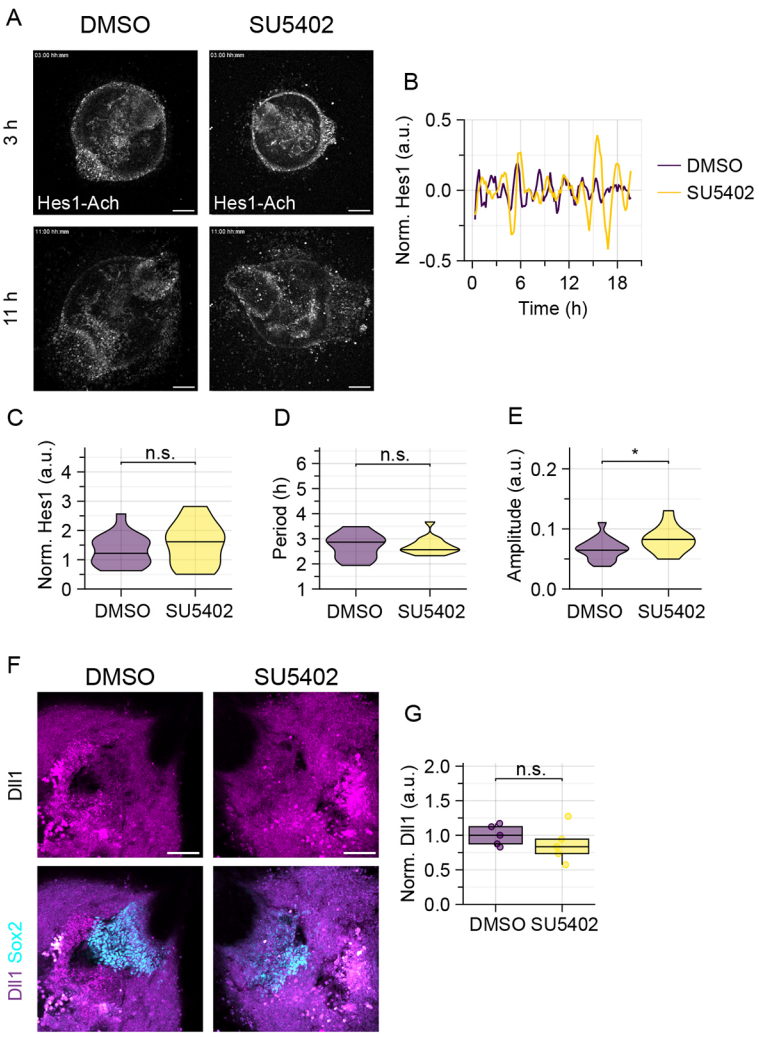

Fig. 6. Induced differentiation by FGF inhibition leads to Hes1 dynamics with increased amplitude. Embryonic tail tips were cultured with DMSO control or the FGF receptor inhibitor SU5402 (20 µM). (A) Representative snapshots of the time series are shown. Scale bars: 100 µm. (B) Representative time series data are shown (all single-cell timeseries data shown in Fig. S9). (C) Quantification of absolute (DMSO-normalized) Hes1-Achilles expression levels (C). (D,E) Quantification of period (D) and amplitude (E) by wavelet transform (0 µM, *n*=15; 20 µM, *n*=15). Further analysis is shown in Fig. S8. (F,G) Cultures were fixed after 21 h and immunostaining against Dll1 and Sox2 was performed. Representative images are shown in F and the quantification is in G (0 µM, *n*=5; 20 µM, *n*=5). Bar indicates the median, boxes indicate the 25th and 75th percentiles, and whiskers indicate 1.5×IQR. Dots in boxplots represent individual data points. Scale bars: 50 µm. **P*<0.05 (Mann–Whitney U-test).

S8N). Thus, this suggests that high FGF signalling levels in pre-NT cells have a dampening effect on Hes1 oscillations and that differentiation leads to an increase in oscillation amplitude, which is not dependent on overall Dll1 protein expression levels.

Inhibiting Notch signalling alters Hes1 dynamics without directly affecting cell proliferation

We next addressed whether a common mechanism drives Hes1 oscillations in cells of the different tissue types. In general, a delayed negative-feedback loop has been suggested to drive oscillations via auto-repression of Hes genes (Goodwin, 1965; Monk, 2003; Takashima et al., 2011; Hirata et al., 2002; Freeman, 2000;Harima et al., 2013; Bessho et al., 2001). In addition to this Hes-driven feedback, the Notch ligand Dll1 is dynamically expressed in the PSM (Shimojo et al., 2016; Takagi et al., 2020), which has been proposed to drive a delayed coupling mechanism between neighbouring cells, resulting in kinematic waves (Takagi et al., 2020; Murray et al., 2013; Morelli et al., 2009; Yoshioka-Kobayashi et al., 2020). In neural tissue, however, Dll1 oscillations were not observed in the pre-NT adjacent to the PSM, but only in the NT adjacent to the last formed somites, where single cells started to oscillate in a salt-and-pepper-like pattern (Shimojo et al., 2016).

To clarify the role of Notch signalling in driving Hes1 oscillations in the embryonic tail, we first analysed the expression of Notch signalling components in the different regions of the embryonic tail, especially the pre-NT. We found Notch ligands Dll1, Dll3 and Dll4, and the Notch receptors to be expressed in the PSM, TB and pre-NT by hybridization chain reaction (Choi et al., 2018) (Fig. S10A,B). We next performed immunostaining to visualize ligand protein expression in the embryonic tail. In agreement with previous publications (Shimojo et al., 2016), Dll1 expression levels were elevated in the PSM compared with the pre-NT, and staining patterns varied between embryonic tails, indicating dynamic expression (Fig. 7A). However, Dll1 – just like Dll4 – was not only detected in the PSM but also in the pre-NT and TB, albeit at lower levels and without indications of dynamics (Fig. 7A). Together with previous findings on Dll1 oscillations in the embryonic tail (Shimojo et al., 2016), this suggests that Dll1 and Dll4 are present at low expression levels in pre-NT cells, whereas Dll1 expression is higher and oscillates in PSM cells, as shown before (Fig. 7B).

To compare the influence of Notch signalling on Hes1 protein dynamics in PSM and pre-NT cells, we inhibited Notch signalling with different doses of DAPT and quantified Hes1-Achilles dynamics within PSM and pre-NT at population level and in single cells (Figs 7, S10 and S11). Analysing dynamics in PSM at population level, we found that Hes1-Achilles expression levels decreased to a similar extent for all DAPT concentrations used (Fig. S10C). The oscillation period was slightly increased at 1 µM DAPT, whereas the amplitude was strongly reduced independently of the DAPT concentration used (Fig. S10D,E). This indicates that,

Development (2024) 151, dev202936. doi:10.1242/dev.202936

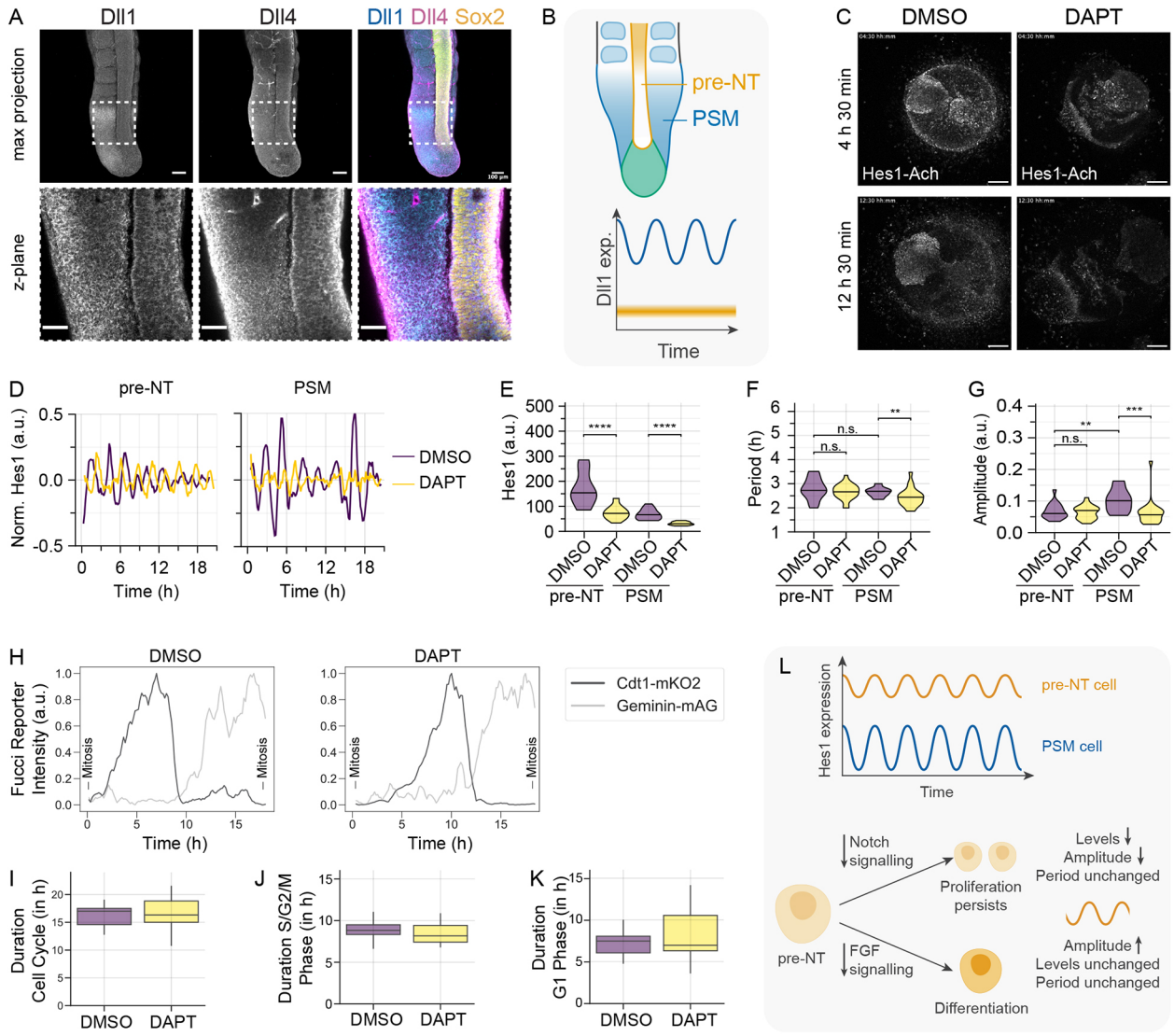

Fig. 7. Notch inhibition has a differential effect on Hes1 oscillations in PSM and pre-NT cells. (A) Representative image of immunostaining of an E10.5 embryonic tail for Dll1, Dll4 and the neural marker Sox2. Scale bars: 100 µm (top); 50 µm (bottom). (B) Schematic illustrating that Dll1 oscillates at high levels in the presomitic mesoderm (PSM), whereas Dll1 levels are low in the preneural tube (pre-NT) and oscillations have not been detected based on previous literature (Shimojo et al., 2016). (C-K) Embryonic 2D spread-out cultures expressing Hes1-Achilles were cultured with DMSO control or the gamma-secretase inhibitor DAPT (10 µM). (C) Representative snapshots of the time series are shown. Scale bars: 100 µm. (D) Representative time series data for pre-NT cells (left panel) and PSM cells (right panel) are shown (all single-cell timeseries data are shown in Fig. S11). (E-G) Quantification of absolute Hes1-Achilles expression levels (E), and period (F) and amplitude (G) by wavelet transform (0 µM *n*=18, 10 µM *n*=21). Further quantification shown in Fig. S8. (H-K) 2D spread-out cultures of embryos showing sparse labelling of the Fucci cell cycle and iRFPnucmem reporters were treated with 10 µM DAPT or DMSO as control. Single cells were tracked and the Fucci reporters based on Cdt1 (G1 phase) and Geminin (S/G2/M phase) were quantified. (H) Representative time series data for DMSO-treated (left panel) and DAPT-treated (right panel) samples are shown. Cell cycle duration (I), duration in S/G2/M phase (J) and duration in G1 phase (K) were analysed (per condition 15 cells from three independent experiments). Bar indicates the median, boxes indicate the 25th and 75th percentiles, and whiskers indicate 1.5×IQR. (L) Schematic highlighting lower Hes1-Achilles expression level and higher Hes1-Achilles amplitude in PSM cells compared with pre-NT cells. In addition, decreasing Notch signalling does not interfere with proliferation in the pre-NT, even though it results in lower Hes1 expression level and amplitude, but leaves the period unchanged. Conversely, induced differentiation by FGF inhibition increases Hes1-Achilles amplitude. ***P*<0.01, ****P*<0.001, *****P*<0.0001 (Mann–Whitney U-test).

at population level, Notch inhibition leads to a loss of Hes1-Achilles oscillations in the PSM, even at low concentrations, which could be consistent with a loss in synchrony between neighbouring cells (Riedel-Kruse et al., 2007). In contrast, in pre-NT (Fig. S10F-H), Notch inhibition led to dose-dependent decrease in Hes1-Achilles expression levels (Fig. S10F) and amplitude (Fig. S10H), whereas no significant change in period was observed (Fig. S10G).

Subsequently, we performed single-cell tracking and quantified Hes1-Achilles expression levels in pre-NT in the different conditions. Also at single-cell level, Notch inhibition led to a dose-dependent decrease of Hes1-Achilles expression levels in pre-NT cells (Figs 7C-E and S10I), whereas the amplitude and period remained unchanged (Figs 7F,G and S10J K). Conversely, in PSM cells Notch inhibition led to a decrease in both Hes1-Achilles expression levels and amplitude (Figs 7C-G and S10L-N). Likewise, the Hes1-Achilles oscillation period was decreased with high DAPT concentration (Fig. 7F). Thus, Notch inhibition has differential effects on Hes1 oscillations in the PSM and pre-NT,

Development (2024) 151, dev202936. doi:10.1242/dev.202936

which implies that the mechanism driving Hes1 dynamics differs between the two cell types.

Although the essential function of Notch signalling in somitogenesis has been studied extensively (Ferjentsik et al., 2009; Ozbudak and Lewis, 2008; Horikawa et al., 2006; Evrard et al., 1998), its role in the pre-NT especially with regards to signalling dynamics is less clear. Notch signalling has been implicated in proliferation control, as overexpression of a dominant-negative form of the Notch ligand Delta1 prevents proliferation (Akai et al., 2005). In other regions of the nervous system, Hes1 oscillations also regulate proliferation with high, sustained Hes1 expression levels promoting quiescence (Marinopoulou et al., 2021; Sueda et al., 2019; Maeda et al., 2023). We therefore addressed how Notch signalling inhibition and a corresponding modulation of Hes1-Achilles dynamics affected pre-NT proliferation. To this end, we inhibited Notch signalling in 2D spread-out cultures expressing the Fucci cell cycle reporter (Sakaue-Sawano et al., 2008). To combine this with mosaic labelling for single-cell tracking, we used a mouse line expressing the inducible nuclear marker iRFPnucmem in the Rosa locus. Comparing control and Notch inhibition, we did not detect differences in the timing of cell cycle, G1 phase, S/G2/M phase or mitosis (Fig. 7H-K). When quantifying the percentage of phospho-histone H3-positive mitotic cells (mitotic index) in the Sox2-positive region, we observed a slight increase in the mitotic index, even at low inhibitor concentrations after 21 h (Fig. S10P,Q). This suggests that lowering Notch signalling per se, which results in decreased Hes1 expression levels and oscillation amplitude but unchanged period, does not affect proliferation in the pre-NT and could indicate that it is instead the dynamics that promote proliferation.

DISCUSSION

Here, we have addressed how Hes dynamics change in the context of the developing embryonic tail, in particular focussing on the tissues derived from NMPs (Fig. 7L). To enable this, we have generated a new endogenous Hes1 reporter mouse line. It contains the fast-maturing fluorescent protein Achilles, which is placed C-terminally to the Hes1 gene. Importantly, the line is homozygously viable and fertile, indicating functionality of the fusion protein, and allows the investigation of Hes1 dynamics at single-cell resolution in various tissue types (Weterings et al., 2024). Using this reporter, we compared Hes1 dynamics in the PSM and pre-NT at population and single-cell level.

To make this feasible, we had to optimize the embryonic tail culture protocol to ensure survival of NT cells during *ex vivo* culture. In contrast to the minimal DMEM-F-12 medium, which is optimal for PSM growth and differentiation (Sonnen et al., 2018), we made use of neurobasal medium that is optimized for culture of neural tissues. The latter is not only supplemented with additional nutrients and vitamins, but also contains proteins such as insulin. Which of these components are required for NT and pre-NT survival must be addressed in future studies. Although this medium allows NT survival, we do observe morphological defects in somite formation, which are presumably due to the presence of retinoic acid in the medium. Despite these morphological defects, the dynamics of the segmentation clock are maintained. This medium therefore allowed us to culture embryonic tails *ex vivo* for the simultaneous quantification of signalling dynamics in both tissues of an embryonic tail.

Differential mechanisms driving Hes1 dynamics in the PSM and pre-NT

In pre-NT cells, Hes1 oscillated at high expression levels with low amplitude, whereas in PSM cells, it oscillated at low expression levels with high amplitude (Fig. 7L). Notch inhibition led to a decrease in Hes1 expression levels and a proportional decrease in the amplitude in pre-NT cells. In contrast, in PSM cells a decrease in amplitude was induced, over-proportional compared with the decrease in Hes1 intensity, both when analysing Hes dynamics at population and single-cell level. This implies that different mechanisms drive Hes1 dynamics in the two tissue types. Although the effect of Notch inhibition in pre-NT cells is consistent with a delayed negative-feedback loop downstream of constant Notch signalling (Goodwin, 1965; Monk, 2003), oscillations in PSM cells appear to be further amplified in a Notch-dependent manner.

In fact, the Notch ligand Dll1 has been shown to oscillate in various cell types, including the PSM, which results in periodic activation of proneural gene expression (Seymour et al., 2020; Shimojo et al., 2016; Zhang et al., 2021). Previously, Dll1 oscillations were not detected in the pre-NT, but only in the NT adjacent to the somites (Shimojo et al., 2016). We have shown here that even in the pre-NT, both Dll1 and Dll4 are present at low expression levels. Interestingly, in a study using cultured cancer cell lines, it was shown that Dll1 expression induces dynamic expression, whereas Dll4 leads to more sustained expression of downstream target genes (Nandagopal et al., 2018). How the presence of each ligand and the dynamics of Dll1 exactly influence Hes1 dynamics in PSM and pre-NT cells has to be addressed in future studies.

In the PSM, oscillatory Dll1 expression has been suggested to lead to kinematic waves travelling through the PSM (Herrgen et al., 2010; Morelli et al., 2009; Shimojo et al., 2016). Loss of Notch-dependant intercellular coupling could therefore explain the loss of population-wide dynamics, which we observed already at low Notch inhibitor concentrations. However, the oscillation amplitude was also reduced in single-cell oscillations upon Notch inhibition, arguing against there being a single effect produced by synchronicity between oscillators. The fact that high Notch inhibitor levels also led to a decrease in the Hes1 oscillation amplitude in the pre-NT at population level suggests that Notch signalling might induce some form of synchronization between pre-NT cells, as suggested recently for Hes5 in the NT (Hawley et al., 2022). Although our mosaic labelling approach for single-cell tracking allows us to track cells and their offspring, it does not allow the quantification of Hes1 dynamics in all neighbours of a given cell. Therefore, the intercellular synchronization between single-cell oscillators has to be addressed in future investigations.

Implications for the role of Hes1 dynamics in the preneural tube

Hes1 dynamics have been found to regulate proliferation and differentiation in the anterior developing NT (Maeda et al., 2023; Kobayashi et al., 2009; Hirata et al., 2002). In undifferentiated cells, Hes1 oscillates in an alternating fashion with proneural genes, while Hes1 is switched off in differentiating cells. Moreover, high absolute expression levels regulate the switch between quiescence and proliferation in adult stem cells, with high expression levels maintaining a quiescent state (Maeda et al., 2023; Marinopoulou et al., 2021; Sueda et al., 2019). It is therefore interesting to note that we find Hes1 expression levels highest in the pre-NT and that expression decreases towards the NT. Moreover, proliferation in the pre-NT requires Notch signalling in chick embryos (Akai et al., 2005). In our experiments, we found that inhibiting Notch signalling, and thereby decreasing Hes1 expression levels and oscillation amplitude, did not change cell cycle timing after 24 h of culture, and perturbation even led to a slight increase in mitotic index. Multiple reasons could explain the apparent discrepancy of

Development (2024) 151, dev202936. doi:10.1242/dev.202936

the role of Notch signalling in the pre-NT. There might be species-specific differences in the requirement for Notch signalling (Cooper et al., 2024). Moreover, based on the remaining Hes1 expression we had detected, we presumably did not inhibit Notch signalling entirely, which might be in contrast to previous studies (Akai et al., 2005). In any case, our data suggest that it might not be the absolute signalling level but the dynamics mediating proliferation control in the pre-NT, as previously suggested for other regions (Maeda et al., 2023; Marinopoulou et al., 2021; Sueda et al., 2019). Although it is compelling to speculate that the Hes1 dynamics remaining upon Notch inhibition are sufficient to allow proliferation, other independent effectors and signals cannot be ruled out.

Not only is expression of Hes1 highest in the pre-NT, but FGF and Wnt signalling are also elevated. High FGF signalling prevents differentiation of the pre-NT to NT (Semprich et al., 2022; Patel et al., 2013; Delfino-Machin et al., 2005; Dubrulle and Pourquie, 2004; Dubrulle et al., 2001). By quantifying Hes1 dynamics in pre-NT cells upon inhibition of FGF signalling, we found that the amplitude of Hes1 dynamics was increased (Fig. 7H). This indicates that FGF has a dampening effect on Hes1 dynamics in the pre-NT and that reduced FGF signalling results in Hes1 dynamics with higher amplitude. Whether FGF signalling directly affects Hes1 dynamics or functions indirectly via induction of differentiation has to be disentangled in the future.

Together, this supports a hypothesis in which cells in the pre-NT are maintained in an undifferentiated, anticipating phase until they become part of the NT, where cells differentiate further in conjunction with the neighbouring somites.

Information transmission by noisy Hes1 oscillations

We have quantified Hes1 oscillations in single PSM, NMP and pre-NT cells. In both NMP and pre-NT cells, Hes1 oscillations are noisy at high expression levels with a low amplitude. In contrast, in the PSM single-cell oscillations are less noisy at low expression levels with a higher amplitude (Fig. 7H). In addition to these single-cell oscillations, it is well known that oscillations between neighbouring PSM cells are coupled, leading to travelling waves of signalling along the tissue (Masamizu et al., 2006; Aulehla et al., 2008; Rohde et al., 2021 preprint). These coupled, highly synchronized oscillations ensure that information for proper segmentation can be transmitted from posterior to anterior in every segmentation cycle.

Even though the pre-NT lies directly adjacent to this oscillating field, the tissues are spatially separated by epithelialization and extracellular material. In the TB and pre-NT, we detect different expression patterns of several signalling components and downstream targets of the Wnt and Notch signalling pathway compared with the PSM (this study and MAMEP database). In correlation with this, Hes1 dynamics in pre-NT cells and NMPs are not only noisy but also less synchronized between neighbouring cells. The absence of synchronized oscillations or travelling waves implies that information in the pre-NT is not transmitted along the anterior-posterior axis via these dynamics. Conversely, Hes1 presumably has a more local function in regulating cellular behaviour on a single-cell basis, as has been suggested in other tissues (Seymour et al., 2020; Zhang et al., 2021).

Notably, once the pre-NT has differentiated to the NT, it has been shown that signalling between somite and NT does regulate further patterning and segmentation of the developing NT in conjunction with the differentiating somite (Kuan et al., 2004). This ensures that spinal cord, nerves and vertebrae form one unit. Thus, proper patterning of the spinal axis of the embryo would be dependent on proper somitogenesis. Based on this, somitogenesis would therefore have to be tightly regulated and coupled to axial elongation, which necessitates highly accurate information transmission. In contrast, differentiation and segmentation of the NT would be downstream of somite formation, which suggests that information could be kept local with the sole aim of allowing proliferation and preventing faulty or premature differentiation of single cells in the pre-NT.

In summary, Notch-dependent Hes1 dynamics in single cells of the developing embryonic tail differ in expression levels, amplitude and noise, which has implications for information transmission in the PSM and NT. The detailed molecular mechanisms through which Hes dynamics are generated and what information is stored in these dynamics in different cell types during embryonic development are important questions for future studies.

MATERIALS AND METHODS

Experimental models

Mouse lines

All animals were housed and bred according to institutional guidelines, and procedures were performed in compliance with Standards for Care and Use of Laboratory Animals with approval from the Hubrecht Institute ethical review board. All animal experiments were approved by the Animal Experimentation Committee (DEC) of the Royal Netherlands Academy of Arts and Sciences.

The Hes1-Achilles knock-in reporter line (Hes1$^{tm1(Link\text{-}Achilles)Kfs}$) was generated by employing CRISPR/Cas9 using IB10 ESCs. To generate Hes1-Achilles alleles, we targeted the stop codon of the endogenous Hes1 locus with a reporter cassette encoding a linked fluorophore (Hes1-linker-Achilles) using the Hes1 gRNA (CGCTCACTTCGGACTCCATG). The reporter cassette is linked to the Hes1 gene via a flexible GSAGS sequence and includes a selection cassette. Briefly, chimeric mice were obtained by C57BL/6 blastocyst injection and then outbred to establish the line through germline transmission. After generation of the knock-in reporter line, the selection cassette was removed by Cre-mediated excision to yield the final Hes1-Achilles allele, using the PGK-Cre mouse line (Lallemand et al., 1998).

The inducible iRFPnucmem mouse line [Gt(ROSA)26Sor$^{tm1(CAG\text{-}iRFPnucmem)Aau}$] was generated by the lab of Alexander Aulehla (EMBL Heidelberg, Germany). iRFPnucmem (Okita et al., 2004; Reimann et al., 2023) was amplified by PCR using the following primers: forward, 5′AGGCCGGCCGCCACCATGGCGG3′; reverse, 5′ TGGCCGGCCTTAGTTTTCC3′. The resulting amplicon was then cloned into the Rosa26 targeting vector Ai9 (Madisen et al., 2010) using the FseI restriction enzyme to generate the loxP-stop-loxP-IRFP713-importin alpha1 construct for conditional expression (Shioi et al., 2011; Abe et al., 2011). The inducible iRFPnucmem mouse line was generated by standard gene targeting techniques using R1 embryonic stem cells. Briefly, chimeric mice were obtained by C57BL/6 blastocyst injection and then outbred to establish the line through germline transmission.

The LuVeLu (Aulehla et al., 2008) and Achilles-Hes7 (Yoshioka-Kobayashi et al., 2020) line were published previously. The R26R-H2B-mCherry (Abe et al., 2011) (‘H2B-mCherry’) and Fucci (Sakaue-Sawano et al., 2008) lines (http://www.clst.riken.jp/arg/reporter_mice.html) were provided by the Riken Center for Biosystems Dynamics Research and Riken BioResource Research Center, respectively (accession numbers CDB0204K, RBRC02706 and RBRC02707). The Tg (T-cre/ERT2)1Lwd/J (Anderson et al., 2013) (‘T-Cre/ERT2’) line was obtained from The Jackson Laboratory (accession number 025520). The Tg (Pgk1-cre)1Lni/CrsJ (Lallemand et al., 1998) (‘PGK-Cre’) line was obtained from the Jackson Laboratory (accession number 020811). The R26-CreERT2 (Ventura et al., 2007) (‘RosaCreERT’) line was obtained from the Jackson Laboratory (accession number 008463).

Cell lines

For the generation of Hes1-Achilles_RosaCreERT ESCs, E3.5 blastocysts were isolated from pregnant Hes1-Achilles_RosaCreERT females. Each blastocyst was transferred to a single well of a 24-well plate seeded with feeder MEFs. After 6 days, cells were trypsinized and expanded into a

Development (2024) 151, dev202936. doi:10.1242/dev.202936

12-well plate with feeders. Four days later, cells were expanded into six-well plates, and simultaneously used for extraction of genomic DNA followed by PCR to determine the genotype. After confirmation of genotype, cells were further expanded for one more passage before freezing down. ESCs were cultured in N2B27-2i medium, as previously described (Silva et al., 2008).

The Sox2-H2B-iRFP ('Sox2-iRFP') knock-in reporter line was generated employing CRISPaint (Schmid-Burgk et al., 2016) gene targeting techniques using Lipofectamine 3000 (ThermoFisher, L3000001) and Hes1-Achilles_RosaCreERT ESCs. To generate Sox2-iRFP alleles, we targeted a PAM site before the stop codon of the endogenous Sox2 locus with a reporter cassette coding for a separated H2B gene linked to a fluorophore (Sox2-T2A-H2B-linker-iRFP) using the Sox2 gRNA (CACTGGAGCTGTCCTTAAATAGG). The reporter cassette was separated from the Sox2 gene via a small 2A sequence. Furthermore, the fluorophore was linked to the H2B gene via a flexible GSAGS sequence. The selection cassette was also separated from the reporter cassette via a small 2A sequence. Selection occurred 2 days after transfection and lasted 3 days. Colonies were picked and transferred to a single well of a 96-well plate seeded with irradiated feeder MEFs. Colonies were then expanded, genotyped and frozen as described above.

Methods details

Transgenic, mouse strains and animal work

Hes1-Achilles mice were genotyped by PCR using the primers Hes1-C-forward (GACCTCGGTGGGTCCTAACGC), linker-Achilles-reverse (CTTGCCGGTGGTGCAGATCAG) and Hes1-N-reverse (GAGGTGGGCTAGGGACTTTACGG). iRFPnucmem mice were genotyped using Rosa-wt-forward (GAGCTGCAGTGGAGTAGGCG), CAG promoter reverse (CTCGACCATGGTAATAGCGA), Rosa-wt-forward (TTGGAGGCAGGAAGCACTTG) and Rosa-wt-reverse (CCGACAAAACCGAAAATCTGTG) primers resulting in the following bands: wild type, 358 bp; 580 bp, transgene.

For all experiments (unless stated otherwise) female mice were euthanized at 10.5 dpc and embryos dissected. Dissections were performed in PBS supplemented with 1% bovine serum albumin (Biowest, P6154), 200 µg penicillin-streptomycin (Gibco, 15140122), 1× GlutaMAX (Gibco, 35050038) and 10% glucose solution 45 (Sigma-Aldrich, G8769). For sparse labelling of mice with H2B-mCherry, iRFPnucmem and Fucci reporters, tamoxifen (Sigma-Aldrich, T5648, dissolved in corn oil) was injected intraperitoneally into pregnant females on day E9.5. For H2B-mCherry and iRFPnucmem, 1 mg and 0.1 mg were used, respectively.

Ex vivo culturing was performed as described previously (Sonnen et al., 2018; Lauschke et al., 2013; Aulehla et al., 2008). The neurobasal medium used to culture *ex vivo* samples consists Special Advanced DMEM/F-12 (Cell Culture Technologies) and Neurobasal medium (Gibco, 12348017) (1:1), 1× N2 (Gibco, 17502048), 1× B27 (Gibco, 12587010), 1× GlutaMAX (Gibco, 35050038), 0.004% bovine serum albumin (Biowest, P6154), 0.1 mM 2-mercaptoethanol and 200 µg penicillin-streptomycin (Gibco, 15140122). The following small molecule inhibitors dissolved in DMSO were used at the concentration indicated in the text and figure legends: FGF-basic ('bFGF', Peprotech, 450-33), CHIR99021 ('Chiron', Sigma-Aldrich, SML1046), DAPT (Sigma-Aldrich, D5942), IWP-2 (Sigma-Aldrich, I0536), retinoic acid (RA; Sigma-Aldrich, R2625-50MG) and SU5402 (Sigma-Aldrich, SML0443). Samples were imaged in eight-well Chambered Coverglass w/non-removable wells (ThermoFisher, 155411PK). Details on resources used can be found in Table S1.

In vitro differentiation

ESCs were differentiated to NMP, mesodermal or neural fate as described previously (Gouti et al., 2014). To minimize fluorescent background, advanced DMEM/F-12 (Cell Culture Technologies) without Phenol Red was used. Cells were differentiated and imaged in µ-Dish 35 mm Quad dishes (Ibidi, 80416).

Translation inhibition and western blotting

To compare protein half-lives of Hes1 wild-type and Hes1-Achilles protein, mESCs heterozygous for Hes1-Achilles were maintained on feeder cells. Two days before the experiments, feeder cells were removed and ESCs cultured in N2B27-2i medium, after which 50 µg/ml cycloheximide (Sigma-Aldrich) or DMSO was added for the indicated amount of time. Cells were harvested and lysed in 2× Laemmli buffer [125 mM Tris-HCl (pH 6.8), 4% SDS, 10% glycerol, 0.2% Bromophenol Blue and 0.05 mM DTT] at 95°Cfor 5 min. Cell numbers were counted to load equal amounts. Proteins were separated in a 12% gel by denaturing polyacrylamide gel electrophoresis (SDS-PAGE) and blotted onto a PVDF membrane as described previously (Sonnen et al., 2013). Western blots were analysed by staining for Hes1 (anti-Hes1 rabbit, clone D6P2U, Cell Signalling Technology, 11988) and alpha-Tubulin (anti-alpha-Tubulin mouse, clone DM1A, Sigma-Aldrich, T6199). Band intensities were quantified using Fiji (Schindelin et al., 2012) and Hes1 levels were quantified by normalizing to the corresponding alpha-Tubulin bands and then to the DMSO control using Python.

RNA interference

To confirm Hes1 antibody specificity in western blotting, knockdown was performed in ESCs. ESCs were cultured on feeder cells. To initiate the experiment, feeder cells were removed and ESCs cultured in N2B27-2i medium. After 1 day of adherent culture, mESCs were transfected with 25 pmol siRNA (Hes1 siRNA #1 GGGAAGUUUAUUUGAGAAAUU, Hes1 siRNA #2 GGAUUGCGCCUUUGUAUUAUU, Hes1 siRNA #3 AGAUCAACGCCAUGACCUAUU; control: GL2 siRNA CGUACGCGGAAUACUUCGAUU) using Lipofectamine RNAiMAX (ThermoFisher, 13778075) according to the manufacturer's instructions. Cells were harvested 72 h after transfection and analysed by western blotting (as described above).

Immunostaining of embryonic tissue

For immunostaining, samples were fixed in 4% formaldehyde for 30 min and kept in PBS at 4°C. Commercial antibodies were used, including anti-Dll1 rat (MABN2284, Sigma-Aldrich), anti-Dll4 goat (AF1389-SP, R&D systems), anti-cleaved caspase 3 rabbit (9661S, CST), anti-phospho Histone H3 mouse (05-806, Sigma-Aldrich), Alexa Fluor 555 Phalloidin (A34055, ThermoFisher), anti-Lyz1 (A0099, DAKO), anti-Tbx6 rabbit (ab38883, Abcam), anti-Sox2 mouse (ab79351, Abcam), anti-Sox2 rabbit (ab92494, Abcam), anti-T human/mouse (AF2085-SP, R&D Systems), anti-Pax6 recombinant (ab195045, Abcam), goat anti-rat Alexa Fluor 555 (A-21434, ThermoFisher), donkey anti-rabbit Alexa Fluor 488 (A-21206, ThermoFisher), donkey anti-rabbit Alexa Fluor 568 (A10042 ThermoFisher), donkey anti-rabbit Alexa Fluor 405 (A48258, ThermoFisher), donkey anti-mouse Alexa Fluor 647 (A-31571, ThermoFisher), donkey anti-rat Alexa Fluor 555 (A78945, ThermoFisher), donkey anti-goat Alexa Fluor 647 (A32849, ThermoFisher), donkey anti-mouse Alexa Fluor 568 (A10037, ThermoFisher) and donkey anti-mouse Alexa Fluor 647 (A-31571, ThermoFisher). We stained samples with primary and secondary antibodies overnight at a 1:1000 dilution in PBST (0.1% Tween 20) containing 1% bovine serum albumin (Biowest, P6154). For imaging, a *z*-stack of 10-12 planes at 10 µm distance was scanned in 1024×1024 pixels (pixel size 0,758 µm) using a Leica TCS SP8 MP confocal microscope.

Immunostaining of small intestine slices

For the characterization of adult tissue in the Hes1-Achilles mice, two males and two virgin females of 8 weeks from both Hes1-linker-Achilles (homozygous) and C57BL/6 background each were used. Small intestine was isolated (from beneath the stomach until the caecum) and immediately flushed with formalin 4%. The tissue was rolled and incubated in formalin 4% for 1 day at room temperature. This was followed by dehydration using a series of ethanol solutions (30%, 50% and 70%). Next, the slides were soaked in xylene, embedded in paraffin wax and sectioned into 5 µm sections. For staining, the slides were soaked in xylene, 100% ethanol, 95% ethanol, 70% ethanol and 50% ethanol, and rinsed with running cold tap water. For antigen retrieval, the slides were cooked in a citrate buffer [sodium citrate (8.2 mM) and citric acid (1.8 mM) at pH 6]. 5% goat serum (ab7481) in 0.3%-Triton X100 PBS was used for blocking and permeabilization. Primary (overnight at 4°C) and secondary antibodies (3 h at room temperature) were used in 0.1%BSA PBS (Lyz1, Dako, A0099,

Development (2024) 151, dev202936. doi:10.1242/dev.202936

1:200). After staining, gut rolls were mounted with Vectashield (H1200NB). The samples were imaged using a SP8 confocal microscope (Leica Microsystems, 40× oil objective, numerical aperture=1.3).

In situ hybridization and hybridization chain reaction

Probe generation and *in situ* hybridization have been described previously (Aulehla et al., 2003). Probes against Axin2, Dusp4, Hes7 and Lfng were used as described in the literature (Aulehla et al., 2003; Mansouri et al., 1997; Saga et al., 1997). Probes against Achilles and Hes1 were generated using the full-length cDNA (Morimoto et al., 2007). Subsequently, samples were dehydrated, embedded in paraffin wax and sectioned. Standard Hematoxylin and Eosin staining was performed.

Hybridization chain reaction was performed as described previously (Choi et al., 2018). Probe sets for the following gene targets: Dll1, Dll3, Dll4, Hes5, Hes7, Meox1, Notch1, Notch2, Notch3, Notch4 and Pax6 were generated (Kuehn et al., 2022). All animals used for hybridization chain reaction were stained once using the same hybridization, washing and amplification time for all gene targets.

Images of *in situ* hybridization were taken with a Leica M165 FC stereomicroscope using 8:1 zoom. Images of hybridization chain reaction were taken with a Leica TCS SP8 MP confocal microscope using a 10× and 20× objective. Brightness and contrast were adjusted uniformly to the entire image.

Confocal real-time microscopy

Real-time imaging was performed using a Leica TCS SP8 MP confocal microscope featuring an incubator and gas mixer for CO_2, O_2 and temperature control. Samples were excited with a OPSL Laser at a wavelength of 514 nm (Hes1-Achilles, Achilles-Hes7 and LuVeLu), 568 nm (H2B-mCherry) or 638 nm (Sox2-iRFP and iRFPnucmem) through a HC PL APO CS2 20×/0.75 DRY objective. For *ex vivo* culture experiments, a *z*-stack of 10-12 planes at 5-10 µm distance was scanned every 10 min. For *in vitro* differentiation experiments, a *z*-stack of three or four planes at 5 µm distance was scanned every 5 min. Multiple samples were recorded using a motorized stage during each experiment. Movies were recorded in 512×512 pixels (pixel size 1517 µm).

Quantification and statistical analysis

Image and data processing

For quantification of mean intensity or number of positive cells in fixed sample imaging, Fiji (Schindelin et al., 2012) was used. For quantification of mitotic cells in spread-out cultures, phospho-histone H3-positive and Sox2-positive cells were counted in the Sox2-positive region using the 'Analyze Particles' function in Fiji and the percentage determined. For quantification of mitotic cells in the embryonic tails, a maximum intensity projection of slices containing the neural tube was made and a region of interest (ROI) outlining the neural tube manually placed. Positive cells were quantified using the 'Analyze Particles' function in Fiji using standard settings (size 50-400 µm^2 and circularity 0.0-1.0). Numbers are displayed as cells per area. Kymographs were generated along the posterior-anterior axis as described previously (Sonnen et al., 2018). For kymographs of embryonic tails, movies were smoothened (gaussian blur, radius 5), a maximum intensity projection was made of slices containing the tissue of interest and movies were registered using the 'Correct 3D drift' function in Fiji. Kymographs were then generated along a 25 pixel-wide line. For quantification of mean intensity over time, ROImanager (quantification of intensity of cell populations), Mastodon (quantification of spot centre intensities for single-cell tracking in spread-out cultures) or manual tracking (quantification of a ROI with 5-15 µm diameter for 2D *in vitro* differentiations) were used.

Data analysis was performed using Julia unless stated otherwise. Quantification of Hes1 intensity was performed as follows: time-courses of cell populations in embryonic tails upon signalling perturbations (Fig. 2 and Fig. S3) were normalized to the starting point of each sample. For quantification of Hes1 intensity in unperturbed embryonic tails or spread-out cultures (Figs 3 and 4), absolute intensity was quantified. Hes1 intensity in spread-out cultures upon signalling perturbations (Figs 6 and 7) was determined by normalizing to the mean of all DMSO samples of each experiment.

Quantification of oscillation dynamics was performed as follows: each time series track was normalized by dividing by its own mean. Tracks were smoothened using rolling average (window size 5). Detrending was performed by determining the trend using rolling average (window size 15) and subtracting this from the smoothened signal. Quantification of oscillation dynamics were performed using pyBOAT (Schmal et al., 2022) implemented in Julia [Settings for wavelet analysis were as follows: global period cutoff for sync-smoothing 225 min, window size for amplitude envelope 450 min, period range from 50 to 350 min (step size 1), window size for ridge detection 45.] For further analysis of period and amplitude, the mean of each track was determined. Fourier transform was obtained from the pyBOAT analysis. For further analysis, peaks with highest power were used (percentile>98). The coefficient of variation was calculated based on these Fourier peaks using the formula cov=std (FourierPeriods)/mean (FourierPeriods).

To quantify synchrony between PSM or NT cells, we calculated the Kuramoto order parameter using python (Sanchez et al., 2022). We first obtained the instantaneous phase of Hes1 dynamics of single cells using pyBOAT (Schmal et al., 2022). The instantaneous phases were used to calculate the instantaneous Kuramoto order parameter of PSM and NT cells per embryo 2D spread-out culture independently. All timepoints were considered, when tracks of at least two cells were available. Last, we extracted the median instantaneous Kuramoto order parameter per tail-tip and cell type as a measure for synchronicity within single tail-tips. Significance was computed using an unpaired Student's *t*-test.

Gut slices were analysed using Fiji (Schindelin et al., 2012), Lyz1-positive cells per crypt were counted manually and graphs were plotted with Prism. To visualize data, Tukey style boxplots were used (bar indicates the median, boxes indicate the 25th and 75th percentiles, and whiskers indicate 1.5×IQR). For statistical comparisons between groups, a Mann–Whitney *U* test was used.

To quantify cell cycle duration in the NT, we tracked single cells carrying Fucci reporters and a mosaically expressed iRFPnucmem. Cell tracks start at a mitotic event and finish at the next mitotic event. Track lengths were used to calculate cell cycle duration. The start of the track until the peak of Cdt1-mKO2 was considered as G1 phase duration, while the peak of Cdt1-mKO2 until the end of the track was considered as S-G2-M duration. To smoothen reporter quantifications, we used a moving average with a window size of five timepoints. In addition, all tracks were min/max normalized between 0 and 1.

Statistical analysis

For all experiments at least three independent experiments were performed. To visualize data, Tukey style boxplots were used (bar indicates the median, boxes indicate the 25th and 75th percentiles, and whiskers indicate 1.5×IQR). Data displayed as violin plots present data from max to min with bar indicating the median. For statistical comparisons between groups, Mann–Whitney *U* tests were computed in Julia, unless stated otherwise.

Acknowledgements

We thank all members of the Sonnen, Bothma and Garaycoechea labs for feedback and discussions. We are thankful to Juan Garaycoechea and Jacques Bothma for feedback on the manuscript. We thank Jan-Daniël de Leede for help with data analysis, Valerie Wilson, Mina Gouti and Jana Wolf for useful discussions, and Andreas Sonnen for help with Alphafold. We thank Jeroen Korving, Stieneke van den Brink, Benaissa el Haddouti, Joris Geigenmüller, Tjerk Swinkels and Mariska Dijkers for technical help. This work was supported by the Hubrecht imaging and animal facilities. The iRFPnucmem mouse line was generated with support from the EMBL Transgenic Core facility (Yvonne Petersen) and mouse facility. We thank Alexander Aulehla for support and providing mouse lines, in particular the inducible iRFPnucmem line. The H2B-mCherry mouse line was kindly provided by the Riken Center for Biosystems Dynamics Research and the Fucci line by the Riken BioResource Research Center. The T-Cre/ERT2, RosaCreERT and PGK-Cre lines were kindly provided by Jackson Laboratories. The LuVeLu reporter line was kindly provided by Olivier Pourquié, the Achilles-Hes7 by Ryoichiro Kageyama and the Achilles construct by Atsushi Miyawaki (Riken Center for Brain Science). The iRFPnucmem construct was kindly provided by Timm Schroeder.

Competing interests

The authors declare no competing or financial interests.

Author contributions

Conceptualization: Y.e.A., P.S., M.S.B., K.F.S.; Methodology: Y.e.A., S.D.C.W., W.H.M.M., W.M.T., K.F.S.; Software: P.S., K.F.S.; Validation: Y.e.A.; Formal analysis: Y.e.A., P.S., M.J.v.O., S.D.C.W., K.F.S.; Investigation: Y.e.A., M.J.v.O., S.D.C.W., K.F.S.; Resources: Y.e.A., N.T.-S.; Data curation: P.S.; Writing - original draft: Y.e.A., K.F.S.; Writing - review & editing: Y.e.A., P.S., M.J.v.O., M.S.B., K.F.S.; Visualization: Y.e.A., P.S., K.F.S.; Supervision: K.F.S.; Project administration: K.F.S.; Funding acquisition: K.F.S.

Funding

P.S. was supported by the KWF Kankerbestrijding (13661). This work was supported by the Hubrecht Institute and received funding from the European Research Council under an ERC starting grant (850554 to K.F.S.). In addition, this research was supported in part by the National Science Foundation (PHY-1748958 to the Kavli Institute for Theoretical Physics). Open Access funding provided by the Hubrecht Institute. Deposited in PMC for immediate release.

Data availability

All relevant data can be found within the article and its supplementary information.

The people behind the papers

This article has an associated 'The people behind the papers' interview with some of the authors.

Peer review history

The peer review history is available online at https://journals.biologists.com/dev/lookup/doi/10.1242/dev.202936.reviewer-comments.pdf

References

Abe, T., Kiyonari, H., Shioi, G., Inoue, K., Nakao, K., Aizawa, S. and Fujimori, T. (2011). Establishment of conditional reporter mouse lines at ROSA26 locus for live cell imaging. *Genesis* **49**, 579-590. doi:10.1002/dvg.20753

Akai, J., Halley, P. A. and Storey, K. G. (2005). FGF-dependent Notch signaling maintains the spinal cord stem zone. *Genes Dev.* **19**, 2877-2887. doi:10.1101/gad.357705

Anderson, M. J., Naiche, L. A., Wilson, C. P., Elder, C., Swing, D. A. and Lewandoski, M. (2013). TCreERT2, a transgenic mouse line for temporal control of Cre-mediated recombination in lineages emerging from the primitive streak or tail bud. *PLoS One* **8**, e62479. doi:10.1371/journal.pone.0062479

Aulehla, A., Wehrle, C., Brand-Saberi, B., Kemler, R., Gossler, A., Kanzler, B. and Herrmann, B. G. (2003). Wnt3a plays a major role in the segmentation clock controlling somitogenesis. *Dev. Cell* **4**, 395-406. doi:10.1016/S1534-5807(03)00055-8

Aulehla, A., Wiegraebe, W., Baubet, V., Wahl, M. B., Deng, C., Taketo, M., Lewandoski, M. and Pourquié, O. (2008). A beta-catenin gradient links the clock and wavefront systems in mouse embryo segmentation. *Nat. Cell Biol.* **10**, 186-193. doi:10.1038/ncb1679

Bansod, S., Kageyama, R. and Ohtsuka, T. (2017). Hes5 regulates the transition timing of neurogenesis and gliogenesis in mammalian neocortical development. *Development* **144**, 3156-3167. doi:10.1242/dev.147256

Bessho, Y., Sakata, R., Komatsu, S., Shiota, K., Yamada, S. and Kageyama, R. (2001). Dynamic expression and essential functions of Hes7 in somite segmentation. *Genes Dev.* **15**, 2642-2647. doi:10.1101/gad.930601

Bessho, Y., Hirata, H., Masamizu, Y. and Kageyama, R. (2003). Periodic repression by the bHLH factor Hes7 is an essential mechanism for the somite segmentation clock. *Genes Dev.* **17**, 1451-1456. doi:10.1101/gad.1092303

Biga, V., Hawley, J., Soto, X., Johns, E., Han, D., Bennett, H., Adamson, A. D., Kursawe, J., Glendinning, P., Manning, C. S. et al. (2021). A dynamic, spatially periodic, micro-pattern of HES5 underlies neurogenesis in the mouse spinal cord. *Mol. Syst. Biol.* **17**, e9902. doi:10.15252/msb.20209902

Bosman, S. L. and Sonnen, K. F. (2022). Signaling oscillations in embryonic development. *Curr. Top. Dev. Biol.* **149**, 341-372. doi:10.1016/bs.ctdb.2022.02.011

Cambray, N. and Wilson, V. (2002). Axial progenitors with extensive potency are localised to the mouse chordoneural hinge. *Development* **129**, 4855-4866. doi:10.1242/dev.129.20.4855

Cambray, N. and Wilson, V. (2007). Two distinct sources for a population of maturing axial progenitors. *Development* **134**, 2829-2840. doi:10.1242/dev.02877

Choi, H. M. T., Schwarzkopf, M., Fornace, M. E., Acharya, A., Artavanis, G., Stegmaier, J., Cunha, A. and Pierce, N. A. (2018). Third-generation in situ hybridization chain reaction: multiplexed, quantitative, sensitive, versatile, robust. *Development* **145**, dev165753. doi:10.1242/dev.165753

Cooper, F., Souilhol, C., Haston, S., Gray, S., Boswell, K., Gogolou, A., Frith, T. J. R., Stavish, D., James, B. M., Bose, D. et al. (2024). Notch signalling influences cell fate decisions and HOX gene induction in axial progenitors. *Development* **151**, dev202098. doi:10.1242/dev.202098

Delfino-Machin, M., Lunn, J. S., Breitkreuz, D. N., Akai, J. and Storey, K. G. (2005). Specification and maintenance of the spinal cord stem zone. *Development* **132**, 4273-4283. doi:10.1242/dev.02009

Dequeant, M. L., Glynn, E., Gaudenz, K., Wahl, M., Chen, J., Mushegian, A. and Pourquie, O. (2006). A complex oscillating network of signaling genes underlies the mouse segmentation clock. *Science* **314**, 1595-1598. doi:10.1126/science.1133141

Dubrulle, J. and Pourquie, O. (2004). fgf8 mRNA decay establishes a gradient that couples axial elongation to patterning in the vertebrate embryo. *Nature* **427**, 419-422. doi:10.1038/nature02216

Dubrulle, J., Mcgrew, M. J. and Pourquie, O. (2001). FGF signaling controls somite boundary position and regulates segmentation clock control of spatiotemporal Hox gene activation. *Cell* **106**, 219-232. doi:10.1016/S0092-8674(01)00437-8

Evrard, Y. A., Lun, Y., Aulehla, A., Gan, L. and Johnson, R. L. (1998). lunatic fringe is an essential mediator of somite segmentation and patterning. *Nature* **394**, 377-381. doi:10.1038/28632

Ferjentsik, Z., Hayashi, S., Dale, J. K., Bessho, Y., Herreman, A., De Strooper, B., Del Monte, G., De La Pompa, J. L. and Maroto, M. (2009). Notch is a critical component of the mouse somitogenesis oscillator and is essential for the formation of the somites. *PLoS Genet.* **5**, e1000662. doi:10.1371/journal.pgen.1000662

Fisher, A. L., Ohsako, S. and Caudy, M. (1996). The WRPW motif of the hairy-related basic helix-loop-helix repressor proteins acts as a 4-amino-acid transcription repression and protein-protein interaction domain. *Mol. Cell. Biol.* **16**, 2670-2677. doi:10.1128/MCB.16.6.2670

Freeman, M. (2000). Feedback control of intercellular signalling in development. *Nature* **408**, 313-319. doi:10.1038/35042500

Goodwin, B. C. (1965). Oscillatory behavior in enzymatic control processes. *Adv. Enzyme Regul.* **3**, 425-438. doi:10.1016/0065-2571(65)90067-1

Gouti, M., Tsakiridis, A., Wymeersch, F. J., Huang, Y., Kleinjung, J., Wilson, V. and Briscoe, J. (2014). In vitro generation of neuromesodermal progenitors reveals distinct roles for wnt signalling in the specification of spinal cord and paraxial mesoderm identity. *PLoS Biol.* **12**, e1001937. doi:10.1371/journal.pbio.1001937

Harima, Y., Takashima, Y., Ueda, Y., Ohtsuka, T. and Kageyama, R. (2013). Accelerating the tempo of the segmentation clock by reducing the number of introns in the Hes7 gene. *Cell Rep.* **3**, 1-7. doi:10.1016/j.celrep.2012.11.012

Hatakeyama, J., Bessho, Y., Katoh, K., Ookawara, S., Fujioka, M., Guillemot, F. and Kageyama, R. (2004). Hes genes regulate size, shape and histogenesis of the nervous system by control of the timing of neural stem cell differentiation. *Development* **131**, 5539-5550. doi:10.1242/dev.01436

Hawley, J., Manning, C., Biga, V., Glendinning, P. and Papalopulu, N. (2022). Dynamic switching of lateral inhibition spatial patterns. *J. R Soc. Interface* **19**, 20220339. doi:10.1098/rsif.2022.0339

Herrgen, L., Ares, S., Morelli, L. G., Schroter, C., Julicher, F. and Oates, A. C. (2010). Intercellular coupling regulates the period of the segmentation clock. *Curr. Biol.* **20**, 1244-1253. doi:10.1016/j.cub.2010.06.034

Hirata, H., Yoshiura, S., Ohtsuka, T., Bessho, Y., Harada, T., Yoshikawa, K. and Kageyama, R. (2002). Oscillatory expression of the bHLH factor Hes1 regulated by a negative feedback loop. *Science* **298**, 840-843. doi:10.1126/science.1074560

Holley, S. A., Julich, D., Rauch, G. J., Geisler, R. and Nusslein-Volhard, C. (2002). her1 and the notch pathway function within the oscillator mechanism that regulates zebrafish somitogenesis. *Development* **129**, 1175-1183. doi:10.1242/dev.129.5.1175

Horikawa, K., Ishimatsu, K., Yoshimoto, E., Kondo, S. and Takeda, H. (2006). Noise-resistant and synchronized oscillation of the segmentation clock. *Nature* **441**, 719-723. doi:10.1038/nature04861

Imayoshi, I. and Kageyama, R. (2014). bHLH factors in self-renewal, multipotency, and fate choice of neural progenitor cells. *Neuron* **82**, 9-23. doi:10.1016/j.neuron.2014.03.018

Jennings, B. H., Pickles, L. M., Wainwright, S. M., Roe, S. M., Pearl, L. H. and Ish-Horowicz, D. (2006). Molecular recognition of transcriptional repressor motifs by the WD domain of the Groucho/TLE corepressor. *Mol. Cell* **22**, 645-655. doi:10.1016/j.molcel.2006.04.024

Jensen, J., Pedersen, E. E., Galante, P., Hald, J., Heller, R. S., Ishibashi, M., Kageyama, R., Guillemot, F., Serup, P. and Madsen, O. D. (2000). Control of endodermal endocrine development by Hes-1. *Nat. Genet.* **24**, 36-44. doi:10.1038/71657

Jumper, J., Evans, R., Pritzel, A., Green, T., Figurnov, M., Ronneberger, O., Tunyasuvunakool, K., Bates, R., Zidek, A., Potapenko, A. et al. (2021). Highly accurate protein structure prediction with AlphaFold. *Nature* **596**, 583-589. doi:10.1038/s41586-021-03819-2

Kobayashi, T. and Kageyama, R. (2010). Hes1 regulates embryonic stem cell differentiation by suppressing Notch signaling. *Genes Cells* **15**, 689-698. doi:10.1111/j.1365-2443.2010.01413.x

Kobayashi, T., Mizuno, H., Imayoshi, I., Furusawa, C., Shirahige, K. and Kageyama, R. (2009). The cyclic gene Hes1 contributes to diverse differentiation responses of embryonic stem cells. *Genes Dev.* **23**, 1870-1875. doi:10.1101/gad.1823109

Kuan, C. Y., Tannahill, D., Cook, G. M. and Keynes, R. J. (2004). Somite polarity and segmental patterning of the peripheral nervous system. *Mech. Dev.* **121**, 1055-1068. doi:10.1016/j.mod.2004.05.001

Kuehn, E., Clausen, D. S., Null, R. W., Metzger, B. M., Willis, A. D. and Ozpolat, B. D. (2022). Segment number threshold determines juvenile onset of germline cluster expansion in Platynereis dumerilii. *J. Exp. Zool. B Mol. Dev. Evol.* **338**, 225-240. doi:10.1002/jez.b.23100

Lallemand, Y., Luria, V., Haffner-Krausz, R. and Lonai, P. (1998). Maternally expressed PGK-Cre transgene as a tool for early and uniform activation of the Cre site-specific recombinase. *Transgenic Res.* **7**, 105-112. doi:10.1023/A:1008868325009

Lauschke, V. M., Tsiairis, C. D., Francois, P. and Aulehla, A. (2013). Scaling of embryonic patterning based on phase-gradient encoding. *Nature* **493**, 101-105. doi:10.1038/nature11804

Lázaro, J., Costanzo, M., Sanaki-Matsumiya, M., Girardot, C., Hayashi, M., Hayashi, K., Diecke, S., Hildebrandt, T. B., Lazzari, G., Wu, J. et al. (2023). A stem cell zoo uncovers intracellular scaling of developmental tempo across mammals. *Cell Stem Cell* **30**, 938-949.e7. doi:10.1016/j.stem.2023.05.014

Madisen, L., Zwingman, T. A., Sunkin, S. M., Oh, S. W., Zariwala, H. A., Gu, H., Ng, L. L., Palmiter, R. D., Hawrylycz, M. J., Jones, A. R. et al. (2010). A robust and high-throughput Cre reporting and characterization system for the whole mouse brain. *Nat. Neurosci.* **13**, 133-140. doi:10.1038/nn.2467

Maeda, Y., Isomura, A., Masaki, T. and Kageyama, R. (2023). Differential cell-cycle control by oscillatory versus sustained Hes1 expression via p21. *Cell Rep.* **42**, 112520. doi:10.1016/j.celrep.2023.112520

Manning, C. S., Biga, V., Boyd, J., Kursawe, J., Ymisson, B., Spiller, D. G., Sanderson, C. M., Galla, T., Rattray, M. and Papalopulu, N. (2019). Quantitative single-cell live imaging links HES5 dynamics with cell-state and fate in murine neurogenesis. *Nat. Commun.* **10**, 2835. doi:10.1038/s41467-019-10734-8

Mansouri, A., Yokota, Y., Wehr, R., Copeland, N. G., Jenkins, N. A. and Gruss, P. (1997). Paired-related murine homeobox gene expressed in the developing sclerotome, kidney, and nervous system. *Dev. Dyn.* **210**, 53-65. doi:10.1002/(SICI)1097-0177(199709)210:1<53::AID-AJA6>3.0.CO;2-0

Marinopoulou, E., Biga, V., Sabherwal, N., Miller, A., Desai, J., Adamson, A. D. and Papalopulu, N. (2021). HES1 protein oscillations are necessary for neural stem cells to exit from quiescence. *iScience* **24**, 103198. doi:10.1016/j.isci.2021.103198

Masamizu, Y., Ohtsuka, T., Takashima, Y., Nagahara, H., Takenaka, Y., Yoshikawa, K., Okamura, H. and Kageyama, R. (2006). Real-time imaging of the somite segmentation clock: revelation of unstable oscillators in the individual presomitic mesoderm cells. *Proc. Natl. Acad. Sci. USA* **103**, 1313-1318. doi:10.1073/pnas.0508658103

Matsuda, M., Yamanaka, Y., Uemura, M., Osawa, M., Saito, M. K., Nagahashi, A., Nishio, M., Guo, L., Ikegawa, S., Sakurai, S. et al. (2020). Recapitulating the human segmentation clock with pluripotent stem cells. *Nature* **580**, 124-129. doi:10.1038/s41586-020-2144-9

Metzis, V., Steinhauser, S., Pakanavicius, E., Gouti, M., Stamataki, D., Ivanovitch, K., Watson, T., Rayon, T., Mousavy Gharavy, S. N., Lovell-Badge, R. et al. (2018). Nervous system regionalization entails axial allocation before neural differentiation. *Cell* **175**, 1105-1118.e17. doi:10.1016/j.cell.2018.09.040

Monk, N. A. (2003). Oscillatory expression of Hes1, p53, and NF-kB driven by transcriptional time delays. *Curr. Biol.* **13**, 1409-1413. doi:10.1016/s0960-9822(03)00494-9

Morales, A. V., Yasuda, Y. and Ish-Horowicz, D. (2002). Periodic Lunatic fringe expression is controlled during segmentation by a cyclic transcriptional enhancer responsive to notch signaling. *Dev. Cell* **3**, 63-74. doi:10.1016/S1534-5807(02)00211-3

Morelli, L. G., Ares, S., Herrgen, L., Schroter, C., Julicher, F. and Oates, A. C. (2009). Delayed coupling theory of vertebrate segmentation. *HFSP J.* **3**, 55-66. doi:10.2976/1.3027088

Morimoto, M., Sasaki, N., Oginuma, M., Kiso, M., Igarashi, K., Aizaki, K., Kanno, J. and Saga, Y. (2007). The negative regulation of Mesp2 by mouse Ripply2 is required to establish the rostro-caudal patterning within a somite. *Development* **134**, 1561-1569. doi:10.1242/dev.000836

Murray, P. J., Maini, P. K. and Baker, R. E. (2013). Modelling Delta-Notch perturbations during zebrafish somitogenesis. *Dev. Biol.* **373**, 407-421. doi:10.1016/j.ydbio.2012.10.014

Nandagopal, N., Santat, L. A., Lebon, L., Sprinzak, D., Bronner, M. E. and Elowitz, M. B. (2018). Dynamic ligand discrimination in the notch signaling pathway. *Cell* **172**, 869-880.e19. doi:10.1016/j.cell.2018.01.002

Niwa, Y., Masamizu, Y., Liu, T., Nakayama, R., Deng, C. X. and Kageyama, R. (2007). The initiation and propagation of Hes7 oscillation are cooperatively regulated by Fgf and notch signaling in the somite segmentation clock. *Dev. Cell* **13**, 298-304. doi:10.1016/j.devcel.2007.07.013

Niwa, Y., Shimojo, H., Isomura, A., Gonzalez, A., Miyachi, H. and Kageyama, R. (2011). Different types of oscillations in Notch and Fgf signaling regulate the spatiotemporal periodicity of somitogenesis. *Genes Dev.* **25**, 1115-1120. doi:10.1101/gad.2035311

Oginuma, M., Takahashi, Y., Kitajima, S., Kiso, M., Kanno, J., Kimura, A. and Saga, Y. (2010). The oscillation of Notch activation, but not its boundary, is required for somite border formation and rostral-caudal patterning within a somite. *Development* **137**, 1515-1522. doi:10.1242/dev.044545

Ohtsuka, T., Ishibashi, M., Gradwohl, G., Nakanishi, S., Guillemot, F. and Kageyama, R. (1999). Hes1 and Hes5 as notch effectors in mammalian neuronal differentiation. *EMBO J.* **18**, 2196-2207. doi:10.1093/emboj/18.8.2196

Ohtsuka, T., Sakamoto, M., Guillemot, F. and Kageyama, R. (2001). Roles of the basic helix-loop-helix genes Hes1 and Hes5 in expansion of neural stem cells of the developing brain. *J. Biol. Chem.* **276**, 30467-30474. doi:10.1074/jbc.M102420200

Okita, C., Sato, M. and Schroeder, T. (2004). Generation of optimized yellow and red fluorescent proteins with distinct subcellular localization. *BioTechniques* **36**, 418-424. doi:10.2144/04363ST01

Ozbudak, E. M. and Lewis, J. (2008). Notch signalling synchronizes the zebrafish segmentation clock but is not needed to create somite boundaries. *PLoS Genet.* **4**, e15. doi:10.1371/journal.pgen.0040015

Palmeirim, I., Henrique, D., Ish-Horowicz, D. and Pourquie, O. (1997). Avian hairy gene expression identifies a molecular clock linked to vertebrate segmentation and somitogenesis. *Cell* **91**, 639-648. doi:10.1016/S0092-8674(00)80451-1

Patel, N. S., Rhinn, M., Semprich, C. I., Halley, P. A., Dolle, P., Bickmore, W. A. and Storey, K. G. (2013). FGF signalling regulates chromatin organisation during neural differentiation via mechanisms that can be uncoupled from transcription. *PLoS Genet.* **9**, e1003614. doi:10.1371/journal.pgen.1003614

Reimann, A., Kull, T., Wang, W., Dettinger, P., Loeffler, D. and Schroeder, T. (2023). Embryonic stem cell ERK, AKT, plus STAT3 response dynamics combinatorics are heterogeneous but NANOG state independent. *Stem Cell Rep.* **18**, 1295-1307. doi:10.1016/j.stemcr.2023.04.008

Riedel-Kruse, I. H., Muller, C. and Oates, A. C. (2007). Synchrony dynamics during initiation, failure, and rescue of the segmentation clock. *Science* **317**, 1911-1915. doi:10.1126/science.1142538

Rohde, L. A., Bercowsky-Rama, A., Valentin, G., Naganathan, S. R., Desai, R. A., Strnad, P., Soroldoni, D. and Oates, A. C. (2021). Cell-autonomous generation of the wave pattern within the vertebrate segmentation clock. *bioRxiv* 2021.05.29.446196. doi:10.1101/2021.05.29.446196

Saga, Y., Hata, N., Koseki, H. and Taketo, M. M. (1997). Mesp2: a novel mouse gene expressed in the presegmented mesoderm and essential for segmentation initiation. *Genes Dev.* **11**, 1827-1839. doi:10.1101/gad.11.14.1827

Sakaue-Sawano, A., Kurokawa, H., Morimura, T., Hanyu, A., Hama, H., Osawa, H., Kashiwagi, S., Fukami, K., Miyata, T., Miyoshi, H. et al. (2008). Visualizing spatiotemporal dynamics of multicellular cell-cycle progression. *Cell* **132**, 487-498. doi:10.1016/j.cell.2007.12.033

Sanchez, P. G. L., Mochulska, V., Mauffette Denis, C., Monke, G., Tomita, T., Tsuchida-Straeten, N., Petersen, Y., Sonnen, K., Francois, P. and Aulehla, A. (2022). Arnold tongue entrainment reveals dynamical principles of the embryonic segmentation clock. *Elife* **11**, e79575. doi:10.7554/eLife.79575

Sasai, Y., Kageyama, R., Tagawa, Y., Shigemoto, R. and Nakanishi, S. (1992). Two mammalian helix-loop-helix factors structurally related to Drosophila hairy and Enhancer of split. *Genes Dev.* **6**, 2620-2634. doi:10.1101/gad.6.12b.2620

Schindelin, J., Arganda-Carreras, I., Frise, E., Kaynig, V., Longair, M., Pietzsch, T., Preibisch, S., Rueden, C., Saalfeld, S., Schmid, B. et al. (2012). Fiji: an open-source platform for biological-image analysis. *Nat. Methods* **9**, 676-682. doi:10.1038/nmeth.2019

Schmal, C., Monke, G. and Granada, A. E. (2022). Analysis of complex circadian time series data using wavelets. *Methods Mol. Biol.* **2482**, 35-54. doi:10.1007/978-1-0716-2249-0_3

Schmid-Burgk, J. L., Honing, K., Ebert, T. S. and Hornung, V. (2016). CRISPaint allows modular base-specific gene tagging using a ligase-4-dependent mechanism. *Nat. Commun.* **7**, 12338. doi:10.1038/ncomms12338

Semprich, C. I., Davidson, L., Amorim Torres, A., Patel, H., Briscoe, J., Metzis, V. and Storey, K. G. (2022). ERK1/2 signalling dynamics promote neural differentiation by regulating chromatin accessibility and the polycomb repressive complex. *PLoS Biol.* **20**, e3000221. doi:10.1371/journal.pbio.3000221

Seymour, P. A., Collin, C. A., Egeskov-Madsen, A. R., Jorgensen, M. C., Shimojo, H., Imayoshi, I., De Lichtenberg, K. H., Kopan, R., Kageyama, R. and Serup, P. (2020). Jag1 Modulates an oscillatory Dll1-Notch-Hes1 signaling module to coordinate growth and fate of pancreatic progenitors. *Dev. Cell* **52**, 731-747.e8. doi:10.1016/j.devcel.2020.01.015

Shimojo, H., Ohtsuka, T. and Kageyama, R. (2008). Oscillations in notch signaling regulate maintenance of neural progenitors. *Neuron* **58**, 52-64. doi:10.1016/j.neuron.2008.02.014

Shimojo, H., Isomura, A., Ohtsuka, T., Kori, H., Miyachi, H. and Kageyama, R. (2016). Oscillatory control of Delta-like1 in cell interactions regulates dynamic gene expression and tissue morphogenesis. *Genes Dev.* **30**, 102-116. doi:10.1101/gad.270785.115

Shioi, G., Kiyonari, H., Abe, T., Nakao, K., Fujimori, T., Jang, C. W., Huang, C. C., Akiyama, H., Behringer, R. R. and Aizawa, S. (2011). A mouse reporter line to conditionally mark nuclei and cell membranes for in vivo live-imaging. *Genesis* **49**, 570-578. doi:10.1002/dvg.20758

Silva, J., Barrandon, O., Nichols, J., Kawaguchi, J., Theunissen, T. W. and Smith, A. (2008). Promotion of reprogramming to ground state

pluripotency by signal inhibition. *PLoS Biol.* **6**, e253. doi:10.1371/journal.pbio.0060253

Sonnen, K. F. and Janda, C. Y. (2021). Signalling dynamics in embryonic development. *Biochem. J.* **478**, 4045-4070. doi:10.1042/BCJ20210043

Sonnen, K. F., Gabryjonczyk, A. M., Anselm, E., Stierhof, Y. D. and Nigg, E. A. (2013). Human Cep192 and Cep152 cooperate in Plk4 recruitment and centriole duplication. *J. Cell Sci.* **126**, 3223-3233. doi:10.1242/jcs.129502

Sonnen, K. F., Lauschke, V. M., Uraji, J., Falk, H. J., Petersen, Y., Funk, M. C., Beaupeux, M., Francois, P., Merten, C. A. and Aulehla, A. (2018). Modulation of phase shift between Wnt and notch signaling oscillations controls mesoderm segmentation. *Cell* **172**, 1079-1090.e12. doi:10.1016/j.cell.2018.01.026

Soza-Ried, C., Ozturk, E., Ish-Horowicz, D. and Lewis, J. (2014). Pulses of Notch activation synchronise oscillating somite cells and entrain the zebrafish segmentation clock. *Development* **141**, 1780-1788. doi:10.1242/dev.102111

Sueda, R., Imayoshi, I., Harima, Y. and Kageyama, R. (2019). High Hes1 expression and resultant Ascl1 suppression regulate quiescent vs. active neural stem cells in the adult mouse brain. *Genes Dev.* **33**, 511-523. doi:10.1101/gad.323196.118

Suzuki, K., Fukui, H., Kayahara, T., Sawada, M., Seno, H., Hiai, H., Kageyama, R., Okano, H. and Chiba, T. (2005). Hes1-deficient mice show precocious differentiation of Paneth cells in the small intestine. *Biochem. Biophys. Res. Commun.* **328**, 348-352. doi:10.1016/j.bbrc.2004.12.174

Takagi, A., Isomura, A., Yoshioka-Kobayashi, K. and Kageyama, R. (2020). Dynamic Delta-like1 expression in presomitic mesoderm cells during somite segmentation. *Gene Expr. Patterns* **35**, 119094. doi:10.1016/j.gep.2019.119094

Takashima, Y., Ohtsuka, T., Gonzalez, A., Miyachi, H. and Kageyama, R. (2011). Intronic delay is essential for oscillatory expression in the segmentation clock. *Proc. Natl. Acad. Sci. USA* **108**, 3300-3305. doi:10.1073/pnas.1014418108

Varadi, M., Bertoni, D., Magana, P., Paramval, U., Pidruchna, I., Radhakrishnan, M., Tsenkov, M., Nair, S., Mirdita, M., Yeo, J. et al. (2024). AlphaFold protein structure database in 2024: providing structure coverage for over 214 million protein sequences. *Nucleic Acids Res.* **52**, D368-D375. doi:10.1093/nar/gkad1011

Ventura, A., Kirsch, D. G., Mclaughlin, M. E., Tuveson, D. A., Grimm, J., Lintault, L., Newman, J., Reczek, E. E., Weissleder, R. and Jacks, T. (2007). Restoration of p53 function leads to tumour regression in vivo. *Nature* **445**, 661-665. doi:10.1038/nature05541

Venzin, O. F. and Oates, A. C. (2020). What are you synching about? Emerging complexity of Notch signaling in the segmentation clock. *Dev. Biol.* **460**, 40-54. doi:10.1016/j.ydbio.2019.06.024

Weterings, S. D. C., Eto, H., de Leede, J.-D., Giladi, A., Hoekstra, M. E., Beijk, W. F., Liefting, E. J. M., van den Anker, K. B., van Rheenen, J., van Oudenaarden, A., Sonnen, K. F. et al. (2024). NOTCH-driven oscillations control cell fate decisions during intestinal homeostasis. *bioRxiv* 2024.08.26.609553. doi:10.1101/2024.08.26.609553

Wu, Y., Liu, Y., Levine, E. M. and Rao, M. S. (2003). Hes1 but not Hes5 regulates an astrocyte versus oligodendrocyte fate choice in glial restricted precursors. *Dev. Dyn.* **226**, 675-689. doi:10.1002/dvdy.10278

Yoshioka-Kobayashi, K., Matsumiya, M., Niino, Y., Isomura, A., Kori, H., Miyawaki, A. and Kageyama, R. (2020). Coupling delay controls synchronized oscillation in the segmentation clock. *Nature* **580**, 119-123. doi:10.1038/s41586-019-1882-z

Zhang, Y., Lahmann, I., Baum, K., Shimojo, H., Mourikis, P., Wolf, J., Kageyama, R. and Birchmeier, C. (2021). Oscillations of Delta-like1 regulate the balance between differentiation and maintenance of muscle stem cells. *Nat. Commun.* **12**, 1318. doi:10.1038/s41467-021-21631-4